PHYSICAL REVIEW D **80,** 076004 (2009)

Supersymmetric dark matter and lepton flavor violation

Vernon Barger,[1,*] Danny Marfatia,[2,†] Azar Mustafayev,[2,‡] and Ali Soleimani[2,§]
[1]*Department of Physics, University of Wisconsin, Madison, Wisconsin 53706, USA*
[2]*Department of Physics & Astronomy, University of Kansas, Lawrence, Kansas 66045, USA*
(Received 11 August 2009; published 16 October 2009)

We study lepton flavor-violating (LFV) processes within a supersymmetric type-I seesaw framework with flavor-blind universal boundary conditions, properly accounting for the effect of the neutrino sector on the dark matter relic abundance. We consider several possibilities for the neutrino Yukawa coupling matrix and show that in regions of SUSY parameter space that yield the correct neutralino relic density, LFV rates can differ from naive estimates by up to 2 orders of magnitude. Contrary to common belief, we find that current LFV limits do not exclude neutrino Yukawa couplings larger than top Yukawa couplings. We introduce the ISAJET-M program that was used for the computations.

DOI: 10.1103/PhysRevD.80.076004 PACS numbers: 11.30.Fs, 12.60.Jv, 13.35.−r, 95.35.+d

I. INTRODUCTION

It is now a firmly established experimental fact that neutrinos are massive and mix [1]. A global fit to current neutrino oscillation data [2] gives the following 3σ ranges/limits for the mixing parameters [in the "standard parametrization," Eq. (A14)],

$$\begin{aligned}
\sin^2\theta_{12} &= 0.304^{+0.066}_{-0.054}, \\
\Delta m^2_{21} &= (7.65^{+0.69}_{-0.60}) \times 10^{-5}\ \text{eV}^2, \\
\sin^2\theta_{23} &= 0.50^{+0.17}_{-0.14}, \\
|\Delta m^2_{31}| &= (2.40^{+0.35}_{-0.33}) \times 10^{-3}\ \text{eV}^2, \\
\sin^2\theta_{13} &< 0.056.
\end{aligned} \tag{1.1}$$

The phases are not constrained by current data.

The most elegant and popular explanation for small neutrino masses is offered by the seesaw mechanism [3]. Here the standard model (SM) is augmented by three right-handed neutrinos (RHNs). The RHNs transform as singlets under the SM gauge group and thus can have a Majorana mass, which is taken to be very large, $M_{\text{Maj}} \sim 10^{15}$ GeV. One of the implications of neutrino mixing is the possibility for charged lepton flavor-violating processes. In the SM-seesaw these rates are highly suppressed by the very large scale M_{Maj} [4], so that LFV processes are a good probe of new physics.

Supersymmetry (SUSY) is a well-motivated possibility for new physics [5,6] because, among other things, it stabilizes the seesaw mechanism [7] and ameliorates the hierarchy problem appearing from the presence of the very high scale M_{Maj} [8]. SUSY must be a broken symmetry that is parametrized by soft SUSY breaking (SSB) terms in the Lagrangian [9]. In general these terms can have arbitrary flavor structures that would induce unacceptably large flavor-violating effects—this is the well-known SUSY flavor problem. The simplest solution is to assume a flavor-blind SUSY breaking mediation mechanism that will generate flavor-universal SSB terms at some high scale. However, this does not mean that SSB terms will also remain flavor universal at the weak scale: flavor-violating terms will be generated by the Yukawa couplings during the evolution from the high to the weak scale. As a consequence, SUSY contributions to LFV processes are suppressed by the characteristic mass scale of SUSY particles $M_{\text{SUSY}} \sim 1$ TeV (instead of M_{Maj}) and thus LFV can be observable. Many authors have studied these processes under various SUSY model assumptions and seesaw parameters (see e.g., [10–19]).

The prediction of LFV rates requires knowledge of the neutrino Yukawa coupling matrix. However, experimentally measured light neutrino masses and mixings do not provide sufficient information to determine it [10]. A top-down approach is frequently adopted in which the neutrino Yukawa matrix is set by a specific SUSY-grand unified theory (GUT), with an $SO(10)$ gauge group being the favorite choice. In this work we take a general approach, and consider two cases of Yukawa unification parameters [defined in Eq. (2.13)] inspired by $SO(10)$ relations. For both of these cases we study two scenarios with small and large mixings in the neutrino Yukawa matrix. Our analysis is based on the type-I seesaw mechanism [3].

The existence of a massive, electrically and color neutral, stable weakly interacting particle that can serve as a cold dark matter (DM) candidate is perhaps the most compelling feature of the R-parity conserving minimal supersymmetric standard model (MSSM). In most cases the DM particle is the lightest neutralino, $\tilde{Z}_1$ [20]. The mass density of DM has been precisely determined by cosmological measurements: a combination of Wilkinson Microwave Anisotropy Probe (WMAP) CMB data with the baryon acoustic oscillations in galaxy power spectra gives

*barger@physics.wisc.edu
†marfatia@ku.edu
‡amustaf@ku.edu
§alis@ku.edu

[21]

$$\Omega_{\rm DM}h^2 = 0.1120^{+0.0074}_{-0.0076} \qquad (2\sigma), \tag{1.2}$$

where $\Omega \equiv \rho/\rho_c$ with ρ_c the critical mass density of the Universe, and h is the scaled Hubble parameter. Such a precise determination places severe constraints on new physics scenarios. In the simplest SUSY model with universal SSB values at the high scale, mSUGRA (or CMSSM) [22], only a few regions of parameter space survive: the bulk region [23,24], the stau [25,26] or stop [27] coannihilation regions, the hyperbolic branch/focus point (HB/FP) region [28], and the A or h resonance annihilation (Higgs funnel) regions [24,29,30]. The benchmark values of mSUGRA input parameters for these regions are listed in Table I.

The introduction of the RHNs and their associated Yukawa couplings changes predictions for some sparticle masses via new contributions to the renormalization group equations (RGEs). These imprints can be used to extract neutrino Yukawa couplings in collider experiments [31]. In previous work [32], some of us demonstrated that these neutrino-induced changes in the SUSY mass spectrum can significantly alter the DM (co)annihilation mechanisms with concomitant changes in $\Omega_{\tilde{Z}_1}h^2$ and DM direct and indirect detection rates.

The aim of the present work is to study predictions for LFV rates while correctly taking into account the aforementioned effect on the neutralino relic density. We take a model-independent approach and only consider effects from RGE running below the unification scale $M_{\rm GUT}$. These two important points distinguish our work (which is closer in spirit to the study of Ref. [11]) from the study of Ref. [33]. We find that proper consideration of the interplay between the neutrino and SUSY sectors can change the predictions for the LFV rates in WMAP-allowed regions by a factor between 2–100 compared with naive estimates, and that contrary to common belief, large neutrino Yukawa couplings are not ruled out by current LFV bounds.

The rest of the paper is organized as follows: In the next section we briefly review LFV processes in SUSY-seesaw framework and motivate our ansatz for the neutrino Yukawa matrix. Results from numerical analyses are presented in Sec. III. Section IV is devoted to the discussion of our findings. Finally, we present our conclusions in Sec. V. Our notation, a description of our code, and Yukawa RGEs with thresholds can be found in the appendices.

TABLE I. Input parameters for benchmark points and corresponding DM-allowed regions of mSUGRA. The dimensionful parameters m_0, $m_{1/2}$, and A_0 are in GeV. For all points $\mu > 0$ and $m_t = 171$ GeV.

Point	m_0	$m_{1/2}$	A_0	$\tan\beta$	Region
A	80	170	−250	10	Bulk
B	100	500	0	10	$\tilde{\tau}$-coan.
C	150	300	−1095	5	$\tilde{t}$-coan.
D	500	450	0	51	A-funnel
E	1370	300	0	10	HB/FP
F	3143	1000	0	10	HB/FP
G	2000	130	−2000	10	h-funnel

II. SUSY-SEESAW AND LFV PROCESSES

We begin with a brief discussion of our formalism. Details about our notation and conventions are relegated to Appendix A. The superpotential for the MSSM augmented by singlet right-handed neutrinos $\hat{N}^c_i$ is

$$\hat{f} = \hat{f}_{\rm MSSM} + (\mathbf{f}_\nu)_{ij}\epsilon_{ab}\hat{L}^a_i\hat{H}^b_u\hat{N}^c_j + \tfrac{1}{2}(\mathbf{M}_N)_{ij}\hat{N}^c_i\hat{N}^c_j, \tag{2.1}$$

where $\hat{f}_{\rm MSSM}$ is the MSSM superpotential shown in Eq. (A1), $\hat{L}$ and $\hat{H}_u$ are, respectively, lepton doublet and up-Higgs superfields, and $\mathbf{M}_N$ represents the Majorana mass matrix for the (heavy) right-handed neutrinos. Above the scale $M_{\rm Maj}$ the light neutrino mass matrix is given by the well-known type-I seesaw formula [3],

$$\mathcal{M}_\nu = -\mathbf{f}_\nu\mathbf{M}_N^{-1}\mathbf{f}_\nu^T v_u^2, \tag{2.2}$$

where v_u is the vacuum expectation value (VEV) of the neutral component h^0_u of the up-type Higgs doublet H_u. At low energies the RHNs decouple from the theory and the light neutrino mass matrix is $\mathcal{M}_\nu = -\kappa v_u^2$. Here, κ is a coupling matrix of the dimension-five effective operator generated by RHNs [see Eq. (A11) for the definition], which is determined by matching conditions (A12) at the RHN decoupling thresholds.

A common solution to the SUSY flavor problem is to assume that at some high scale sfermion SSB mass-squared matrices are diagonal and universal in flavor, and the trilinear couplings are proportional to the Yukawa couplings. In the framework of mSUGRA extended by right-handed neutrinos (mSUGRA seesaw) the SSB boundary conditions at grand unification scale $M_{\rm GUT}$ take the particularly simple form

$$\begin{gathered}\mathbf{m}^2_{\mathbf{Q},\mathbf{U},\mathbf{D},\mathbf{L},\mathbf{E},\tilde{\nu}_\mathbf{R}} = m_0^2\mathbb{1}, \qquad m^2_{H_u} = m^2_{H_d} = m_0^2, \\ \mathbf{a}_{u,d,e,\nu} = -A_0\mathbf{f}_{u,d,e,\nu}.\end{gathered} \tag{2.3}$$

Since the Yukawa couplings $\mathbf{f}_e$ and $\mathbf{f}_\nu$ cannot be simultaneously diagonalized, nonvanishing off-diagonal elements will be generated in the left-handed slepton mass matrix $\boldsymbol{m}^2_{\tilde{L}}$ via renormalization group evolution. In the leading-logarithmic approximation with universal boundary conditions (2.3) the off-diagonal elements are

$$(\boldsymbol{m}^2_{\tilde{L}})_{i\neq j} \simeq -\frac{1}{8\pi^2}(3m_0^2 + A_0^2)\sum_k (\mathbf{f}^T_\nu)_{ik}(\mathbf{f}^*_\nu)_{kj}\log\frac{M_{\rm GUT}}{M_{N_k}}, \tag{2.4}$$

where M_{N_k} are RHN decoupling scales that are approximately equal to the eigenvalues of the Majorana mass

matrix $\mathbf{M}_N$. At low energies, these off-diagonal terms induce LFV processes such as $l_i \to l_j\gamma$, $l_i \to 3l_j$ and $l_i \to l_j$ conversion in nuclei. Current bounds on LFV processes as well as the projected sensitivities of future experiments are summarized in Table II.

The branching ratio for the flavor-violating radiative decay of a charged lepton is given by

$$\mathrm{BR}(l_i \to l_j\gamma) = \frac{\alpha}{4\Gamma(l_i)} m_{l_i}^5 (|A_L|^2 + |A_R|^2). \tag{2.5}$$

Here, α is the electromagnetic fine structure constant, $\Gamma(l_i)$ is the total decay width of the initial lepton, and $A_{L,R}$ are form factors for left and right chiralities of the incoming lepton whose full expressions in SUSY were obtained in Ref. [12]. Because $m_{l_i} \gg m_{l_j}$ one has $A_R \gg A_L$ in the case of initial universality such as (2.3) [10,13]. In the mass-insertion approximation, the branching ratio can be related to the corresponding off-diagonal element of the left-handed slepton mass matrix [13],

$$\mathrm{BR}(l_i \to l_j\gamma) \simeq \mathrm{BR}(l_i \to l_j\bar{\nu}_j\nu_i) \frac{\alpha^3}{G_F^2 m_s^8} |(\boldsymbol{m}_L^2)_{i\neq j}|^2 \tan^2\beta, \tag{2.6}$$

where G_F is the Fermi coupling constant and m_s is the characteristic mass scale of the SUSY particles in the loop. In the case of universal boundary conditions (2.3), this expression used in conjunction with the leading-log result (2.4) well approximates the full expression (2.5), if one sets [14]

$$m_s^8 \simeq 0.5 m_0^2 m_{1/2}^2 (m_0^2 + 0.6 m_{1/2}^2)^2. \tag{2.7}$$

LFV $l_i \to 3l_j$ decays and $l_i \to l_j$ conversion occur via γ, Z, and Higgs penguins as well as squark/slepton box diagrams [12]. Higgs penguins dominate in the regime of large $\tan\beta \simeq 60$ and light H/A Higgs boson mass $\sim$100 GeV, and enhance rates by up to a few orders of magnitude [15]. However, the latter condition cannot be realized in the universal scenario (2.3) [45]. It was shown in Ref. [16] that these LFV rates are well described in the universal scenario by the same γ penguins that contribute to the radiative decays. The branching ratio for trilepton decays is approximately given by

$$\mathrm{BR}(l_i \to 3l_j) \simeq \frac{\alpha}{3\pi}\left(\log\frac{m_{l_i}^2}{m_{l_j}^2} - \frac{11}{4}\right)\mathrm{BR}(l_i \to l_j\gamma). \tag{2.8}$$

For $\mu \to e$ conversion a similar relation holds:

$$\mathrm{CR}(\mu N \to eN) \equiv \frac{\Gamma(\mu N \to eN)}{\Gamma_{\mathrm{capt}}} = \frac{16\alpha^4 Z}{\Gamma_{\mathrm{capt}}} Z_{\mathrm{eff}}^4 |F(q^2)|^2 \mathrm{BR}(\mu \to e\gamma), \tag{2.9}$$

where Z is the proton number of the nucleus N, Z_{eff} is an effective atomic charge obtained by averaging the muon wave function over the nuclear density [46], $F(q^2)$ denotes the nuclear form factor at momentum transfer q [47] and Γ_{capt} is the measured total muon capture rate [48]. In this work we consider two target materials that will be used by future experiments. For $^{48}_{22}$Ti, which will be used by the proposed PRIME experiment at J-PARC [43], $Z_{\mathrm{eff}} = 17.6$, $F(q^2 \simeq -m_\mu^2) \simeq 0.54$ and $\Gamma_{\mathrm{capt}} = 2.590 \times 10^6$ sec^{-1}. For $^{27}_{13}$Al, the target material for the proposed Mu2e experiment at Fermilab [44], $Z_{\mathrm{eff}} = 11.48$, $F(q^2 \simeq -m_\mu^2) \simeq 0.64$ and $\Gamma_{\mathrm{capt}} = 7.054 \times 10^5$ sec^{-1}.

TABLE II. Present bounds and projected sensitivities for LFV processes.

	Present	Future
BR($\mu \to e\gamma$)	1.2×10^{-11} [34]	10^{-13} [35]
BR($\tau \to \mu\gamma$)	4.5×10^{-8} [36]	10^{-9} [37]
BR($\tau \to e\gamma$)	3.3×10^{-8} [38]	10^{-9} [37]
BR($\mu \to eee$)	1.0×10^{-12} [39]	10^{-14} [40]
BR($\tau \to \mu\mu\mu$)	3.2×10^{-8} [41]	10^{-9} [37]
BR($\tau \to eee$)	3.6×10^{-8} [41]	10^{-9} [37]
CR(μTi $\to e$Ti)	4.3×10^{-12} [42]	10^{-18} [43]
CR(μAl $\to e$Al)	-	10^{-16} [44]

SO(10) GUTs

As discussed in the previous section, LFV rates crucially depend on the neutrino Yukawa coupling matrix $\mathbf{f}_\nu$. However, this matrix cannot be reconstructed from experimental data by inverting the seesaw formula (2.2): $\mathbf{f}_\nu$ and $\mathbf{M}_N$ together depend on 18 parameters, while $\mathcal{M}_\nu$ contains only 9 observables. A common solution is to turn to GUTs where $\mathbf{f}_\nu$ is related to the known Yukawa matrices of SM fermions.

$SO(10)$ GUTs unify all SM fermions and the right-handed neutrino of each generation in a single **16**-dimensional spinor representation. The Higgs representation assignments are determined by the following decompositions of the direct products

$$\mathbf{16} \otimes \mathbf{16} = \mathbf{10} \oplus \mathbf{120} \oplus \mathbf{126}, \tag{2.10}$$

$$\mathbf{16} \otimes \overline{\mathbf{16}} = \mathbf{1} \oplus \mathbf{45} \oplus \mathbf{210}. \tag{2.11}$$

Many $SO(10)$ models exist in the literature with different choices of Higgs representations and, frequently, with additional flavor symmetries. These models can be divided in two general classes [49]. The first uses only low dimensional Higgs multiplets **10**, **16**, **45** with some nonrenormalizable operators constructed from them. This necessarily leads to large R-parity violation so that these models cannot provide a DM candidate. Models in the other class involve **10**, **120**, or **126** Higgs representations, have renormalizable couplings, preserve R-parity, and are often referred to as minimal Higgs models. The resulting set of sum rules for the mass matrices are

$$\begin{aligned}
\mathbf{f}_u v_u &= \mathbf{f}_{10} v_u^{10} + \mathbf{f}_{126} v_u^{126} + \mathbf{f}_{120} v_u^{120},\\
\mathbf{f}_d v_d &= \mathbf{f}_{10} v_d^{10} + \mathbf{f}_{126} v_d^{126} + \mathbf{f}_{120} v_d^{120},\\
\mathbf{f}_e v_d &= \mathbf{f}_{10} v_d^{10} - 3\mathbf{f}_{126} v_d^{126} + \mathbf{f}_{120} v_d^{120},\\
M_{\nu,LR} \equiv \mathbf{f}_\nu v_u &= \mathbf{f}_{10} v_u^{10} - 3\mathbf{f}_{126} v_u^{126} + \mathbf{f}_{120} v_u^{120},\\
M_{\nu,RR} \equiv \mathbf{M}_N &= \mathbf{f}_{126} V_R, \qquad M_{\nu,LL} = \mathbf{f}_{126} v_L, \qquad (2.12)
\end{aligned}$$

where $\mathbf{f}_{\mathcal{R}}$ are $SO(10)$ Yukawa coupling matrices, $v_{u,d}^{\mathcal{R}}$ are VEVs of the various $SU(2)_L$ doublets (with Higgs fields residing in $\mathcal{R} \equiv \mathbf{10}, \mathbf{126}, \mathbf{120}$), and v_L and V_R are the $B-L$ breaking VEVs of the $SU(2)_L$ triplet and singlet, respectively. In the type-I seesaw, which we consider in this paper, $v_L = 0$ and SUSY prevent its reappearance via loop diagrams [7].

From Eq. (2.12), if Higgs superfields reside in **10**, as they do in the simplest scenarios, then the neutrino Yukawa matrix will be identical to the up-quark Yukawa at $M_{\rm Gut}$. If the Higgses are in **126**, then $\mathbf{f}_\nu = -3\mathbf{f}_u$. A dominant **120** Higgs would lead to at least a pair of degenerate heavy up-quarks [50] and thus is phenomenologically excluded. Motivated by the above, we introduce a *neutrino Yukawa unification parameter* as

$$\mathbf{f}_\nu \propto R_{\nu u} \mathbf{f}_u, \qquad (2.13)$$

and consider two cases,[1] $|R_{\nu u}| = 1$ and $|R_{\nu u}| = 3$. Note that $\mathbf{f}_\nu$ and $\mathbf{f}_u$ need not be aligned: the subdominant contributions from other Higgs multiplets and/or flavor group structure can lead to different diagonalization matrices. To keep our discussion as simple as possible, we consider two extreme cases of the mixing present in $\mathbf{f}_\nu$.

Large mixing: The measured values of the neutrino mixing angles (1.1) are consistent with the so-called tribimaximal pattern [51,52], where $\sin^2\theta_{12} = \frac{1}{3}$, $\sin^2\theta_{23} = \frac{1}{2}$, $\sin^2\theta_{13} = 0$. Thus, it is reasonable to postulate that mixing in the neutrino Yukawa matrix at the GUT scale also has a tribimaximal form. In other words, we assume that the observed Maki-Nakagava-Sakata (MNS) mixing matrix arises only from the left-handed rotation matrix (i.e., we set $\mathbf{V}_{\nu_R} = \mathbb{1}$). We take a neutrino Yukawa matrix of the form[2]

$$\mathbf{f}_\nu = R_{\nu u} \mathbf{V}_{\nu_L} \mathbf{f}_u^{\rm diag}, \qquad (2.14)$$

with

$$\mathbf{V}_{\nu_L}^\dagger = \mathbf{U}_\nu^\dagger = \begin{pmatrix} \sqrt{\frac{2}{3}} c_\chi c_\phi + i\sqrt{\frac{2}{3}} s_\chi s_\phi & \frac{1}{\sqrt{3}} & -\sqrt{\frac{2}{3}} c_\chi s_\phi - i\sqrt{\frac{2}{3}} s_\chi c_\phi \\ -\frac{c_\chi c_\phi + i s_\chi s_\phi}{\sqrt{6}} - \frac{c_\chi s_\phi - i s_\chi c_\phi}{\sqrt{2}} & \frac{1}{\sqrt{3}} & -\frac{c_\chi c_\phi - i s_\chi s_\phi}{\sqrt{2}} + \frac{c_\chi s_\phi + i s_\chi c_\phi}{\sqrt{6}} \\ -\frac{c_\chi c_\phi + i s_\chi s_\phi}{\sqrt{6}} + \frac{c_\chi s_\phi - i s_\chi c_\phi}{\sqrt{2}} & \frac{1}{\sqrt{3}} & \frac{c_\chi c_\phi - i s_\chi s_\phi}{\sqrt{2}} + \frac{c_\chi s_\phi + i s_\chi c_\phi}{\sqrt{6}} \end{pmatrix}, \qquad (2.15)$$

where $s_\chi = \sin\chi$, $c_\chi = \cos\chi$, $s_\phi = \sin\phi$, $c_\phi = \cos\phi$, and the parameters χ, $\phi \in [0, 2\pi]$. This is the simplest generalization of a tribimaximal mixing ($\chi = \phi = 0$) that allows CP violation [52]. A fit to experimental values (1.1) reveals that the Harrison-Scott parameters χ and ϕ are restricted to the vicinity of $\chi + \phi \simeq n\pi$, with the upper bound on θ_{13} imposing the strongest constraint. Ignoring RGE effects, we invert the seesaw formula and obtain the approximate form for the Majorana mass matrix

$$\mathbf{M}_N \simeq {\rm diag}\left(\frac{m_u^2}{m_{\nu_1}}, \frac{m_c^2}{m_{\nu_2}}, \frac{m_t^2}{m_{\nu_3}}\right) \times R_{\nu u}^2. \qquad (2.16)$$

We will consider this case as representative of the large mixing scenario.

Small mixing: For the small mixing scenario, we take the neutrino and up-quark Yukawa matrices to be exactly aligned with each other at the GUT scale,

$$\mathbf{f}_\nu = R_{\nu u} \mathbf{f}_u, \qquad (2.17)$$

so that neutrino mixing is given by the Cabibbo-Kobayashi-Maskawa (CKM) matrix. Then, in the absence of significant RGE magnification effects, the Majorana mass matrix cannot be diagonal. Assuming tribimaximal mixing in $\mathcal{M}_\nu$ and neglecting the small mixing in $\mathbf{f}_\nu$ we can estimate eigenvalues $\mathbf{M}_N$ for the normal hierarchy of light neutrinos ($m_{\nu_1} \ll m_{\nu_2} \ll m_{\nu_3}$),

$$M_{N_1} \simeq \frac{3m_u^2}{m_{\nu_2}} R_{\nu u}^2, \qquad M_{N_2} \simeq \frac{2m_c^2}{m_{\nu_3}} R_{\nu u}^2, \qquad M_{N_3} \simeq \frac{m_t^2}{6m_{\nu_1}} R_{\nu u}^2. \qquad (2.18)$$

For the inverted mass hierarchy ($m_{\nu_1} \simeq m_{\nu_2} \gg m_{\nu_3}$), a similar procedure yields

$$M_{N_1} \simeq \frac{3m_u^2}{m_{\nu_2}} R_{\nu u}^2, \qquad M_{N_2} \simeq \frac{2m_c^2}{3m_{\nu_1}} R_{\nu u}^2, \qquad M_{N_3} \simeq \frac{m_t^2}{2m_{\nu_3}} R_{\nu u}^2. \qquad (2.19)$$

Notice that the largest RHN mass is controlled by the smallest light neutrino mass.

From Eqs. (2.16), (2.17), (2.18), and (2.19), we see that RHNs have a very strong mass hierarchy "quardatic" to the one in up-quark sector $M_{N_1}:M_{N_2}:M_{N_3} \sim m_u^2:m_c^2:m_t^2$. For this reason, only the spectrum with normal hierarchy of light neutrinos is feasible. A quasidegenerate spectrum ($m_{\nu_1} \simeq m_{\nu_2} \simeq m_{\nu_3}$) would require the lightest Majorana mass to be in the 10^2–10^3 GeV range with significant

[1] Henceforth, we denote $|R_{\nu u}|$ by $R_{\nu u}$.

[2] This corresponds to trivial misalignment matrix $\mathbf{R} = \mathbb{1}$ in the Casas-Ibarra parametrization [10].

L-R mixing in the sneutrino sector, which is in conflict with our approximations [see the discussion pertaining to Eq. (A15)]. Moreover, such light Majorana masses make successful thermal leptogenesis impossible. The inverse hierarchical case would require the heaviest Majorana mass to be of order 10^{17} GeV, which is well above the GUT scale. This type of spectrum also suffers instabilities under very small changes to $\mathbf{M}_N$ and RGE evolution [53]. In the rest of the paper we concentrate on the normal hierarchy case, which is also favored by GUT model building [54].

III. PROCEDURE AND RESULTS

We extensively modified ISAJET [55] by including the neutrino sector and by implementing RGE evolution in matrix form to incorporate flavor effects in both the quark and lepton sectors. The resulting program ISAJET-M performs RGE evolution in the MSSM augmented with RHNs at 2-loop level taking into account various thresholds and computes sparticle spectra including radiative corrections. The computation of the neutralino relic density is done using the IsaReD code [26] and LFV rates are computed using the full one-loop formulae from Ref. [12]. A graphical outline of our procedure is presented in Fig. 1, and details of the program are provided in Appendix B.

In the neutrino sector we employ a "top-down" approach in which $\mathbf{f}_\nu$ and $\mathbf{M}_N$ are inputs at the scale $M_{\rm Gut}$. Physical neutrino masses and mixings are derived results, which we require to be within the experimental bounds (1.1). We consider the two cases for neutrino Yukawa

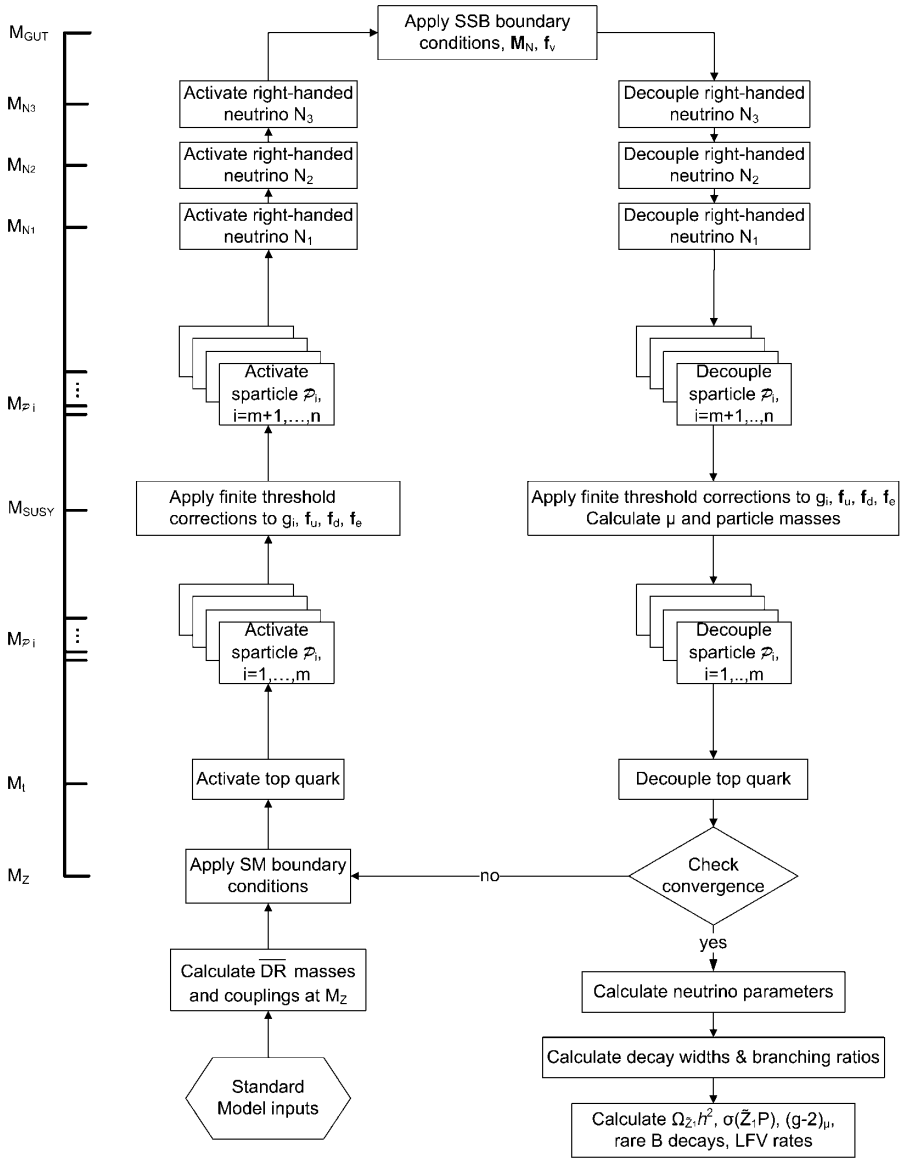

FIG. 1. Code flowchart. $\mathcal{P}_i$ represent sparticles and Higgses arranged in the ascending order of their masses. The code is described in Appendix B.

unification parameter, $R_{\nu u} = 1$ and $R_{\nu u} = 3$, which were introduced earlier. For each case we consider scenarios with large and small neutrino mixings using Eqs. (2.14) and (2.17) to set the neutrino Yukawa matrix at $M_{\rm Gut}$. This also restricts Majorana masses to be below that scale, i.e. $\max(M_{N_i}) \lesssim M_{\rm Gut}$.

In the quark sector we choose a basis at the weak scale in which CKM rotation is entirely in the up-quark sector: we set the fermion rotation matrices (A3) to be $\mathbf{V}_{\mathbf{u_L}} = \mathbf{V}_{\mathbf{u_R}} = \mathbf{V}_{\rm CKM}$ and $\mathbf{V}_{\mathbf{d_L}} = \mathbf{V}_{\mathbf{d_R}} = \mathbb{1}$. Note that this does not mean that $\mathbf{f}_d$ remains diagonal at all scales—off-diagonal terms will be generated at higher scales due to RGE effects. Similarly, for charged leptons we set $\mathbf{V}_{\mathbf{e_L}} = \mathbf{V}_{\mathbf{e_R}} = \mathbb{1}$ at M_Z.

Regarding the SUSY sector we work in the well-studied scenario specified by the parameter set

$$m_0, \qquad m_{1/2}, \qquad A_0, \qquad \tan\beta, \qquad \mathrm{sgn}(\mu), \tag{3.1}$$

where GUT-scale boundary conditions are universal and defined by Eq. (2.3). This choice of boundary conditions is frequently referred to as mSUGRA-like. Instead of scanning over the full parameter space, which would be exceedingly computational intensive, we study specific points for each DM-allowed region. Throughout this work we take $\mu > 0$ as suggested by measurements of the muon anomalous magnetic moment [56–58] and set the pole mass of top quark $m_t = 171$ GeV in accord with Tevatron data [59]. For the DM relic density, we consider the conceptually simplest scenario in which the DM is comprised only of the lightest neutralino $\tilde{Z}_1$ that is thermally produced in the standard ΛCDM cosmology. We first calculate the neutralino relic density (RD) and LFV rates in our framework *with* SUSY seesaw using points from Table I that have WMAP-allowed values in the mSUGRA framework *without* seesaw—a procedure commonly used in the literature. Then, if the RD turns out to be too high, as is frequently the case, we find new points consistent with the WMAP range (1.2) by adjusting SSB parameters and calculate the corresponding LFV rates.

A. Large mixing

We begin by considering the $R_{\nu u} = 1$ case. Numerically we find that the GUT-scale Majorana mass matrix

$$\mathbf{M}_N = \mathrm{diag}(4.75\times10^{-6}, 4.75\times10^{-5}, 1)\times 1.398 \times 10^{14}\ \mathrm{GeV} \tag{3.2}$$

produces the spectrum $m_{\nu_1} \sim 10^{-5}$ eV, $m_{\nu_2} \simeq \sqrt{\Delta m^2_{21}} \simeq 8\times10^{-3}$ eV, and $m_{\nu_3} \simeq \sqrt{\Delta m^2_{31}} \simeq 5\times10^{-2}$ eV, which is in accord with experimental limits (1.1). We chose the mass of the lightest RHN to be far above $M_{\rm SUSY}$ to prevent the unwanted mixing in the sneutrino sector. Equation (3.2) is in good agreement with our estimate (2.16) up to a factor of $\sim$2 reduction of up-quark Yukawa couplings (see, for example, Ref. [60]) due to the RGE effects. This is because $\mathbf{f}_\nu$, $\mathbf{M}_N$, and the spectrum of light neutrinos are hierarchical and as such experience very little change in RGE evolution [61].

In the Harrison-Scott parameterization (2.15), that we use for the mixing in the neutrino Yukawa matrix at the GUT scale, the Dirac phase δ and mixing angles are a function of ϕ and χ. $\delta = \pi/2$ for $\phi = 0$ see the left frame of Fig. 2. It is known that LFV rates depend on the value of the unknown Dirac phase [16]. In addition, most LFV rates are very sensitive to the value of θ_{13} [17] for which only an upper bound exists. To quantify these dependences, in the middle frame of Fig. 2 we show the branching ratio for $\mu \to e\gamma$ as a function of the Harrison-Scott parameters. We present them as enhancement factors relative to the rates at $\{\phi, \chi\} = \{0, 0.294\}$ for which $\theta_{13} = 0.239$ (or $\sin^2\theta_{13} = 0.056$) and $\delta = \pi/2$. We see that with θ_{13} fixed, the branching ratio changes by up to $\sim$35% under variation of δ. The dependence on θ_{13} is greater and more complex: rates change by about 2 orders of magnitude for θ_{13} ranging from 0.239 to 0.045 (or $\sin^2 2\theta_{13} = 0.008$), with the latter being the ultimate reach of the Daya Bay experiment [62]. Closer to $\phi = \chi = 0$, the rates change much faster and drop by several more orders of magnitude. The rates for the other θ_{13}-dependent LFV processes follow the same pattern as expected from Eqs. (2.8) and (2.9). On the other hand, rates for $\tau \to \mu\gamma$ and $\tau \to 3\mu$ are relatively independent of θ_{13} [17]. In the right frame of Fig. 2 we show enhancement factor contours for $\tau \to \mu\gamma$. We see that rates change with θ_{13} by only $\sim$13%: this variation is an artifact of the paramterization (2.15), in which $\sin^2\theta_{12} = 0.33/\cos^2\theta_{13}$. Also variation with respect to δ is smaller—only up to $\sim$10%. We numerically confirmed that $\tau \to 3\mu$ rates behave similarly, as expected from Eq. (2.8).

In Figs. 3–6, we show the LFV rates along with current experimental bounds (horizontal dashed lines) and projected future sensitivities (dash-dotted lines). To account for the aforementioned dependences on θ_{13} and δ, we show rates for $\{\phi, \chi\} = \{0, 0.294\}$ (for which $\sin^2\theta_{13} = 0.056$ and $\delta = \pi/2$) as diagonally hatched bars and for $\phi = \chi = 0$ (resulting in $\sin^2\theta_{13} = 0$) as solid bars. We also present rates for $\{\phi, \chi\} = \{0, 0.022\}$ (giving $\sin^2\theta_{13} = 0.002$ and $\delta = \pi/2$) as cross-hatched bars to indicate the upper limit on the rates if the Daya Bay [62] and Double Chooz [63] experiments produce a null result.

In the bulk [23,24] and the stau-coannihilation [25,26] regions, the neutralino RD is within the WMAP range due to $\tilde{Z}_1$ interactions with the lighter stau $\tilde{\tau}_1$. Under universal boundary conditions $\tilde{\tau}_1$ is a dominantly right-handed state and as such remains unaffected by the neutrino Yukawa coupling.[3] Therefore, the use of mSUGRA values (points *A* and *B*) in models with RHNs still produces the correct RD.

[3]A detailed discussion of neutrino Yukawa coupling effects on SUSY spectrum and DM observables can be found in Ref. [32].

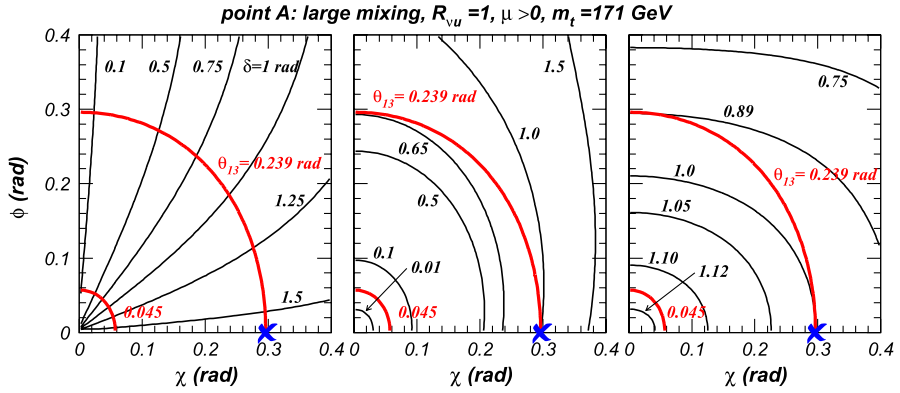

FIG. 2 (color online). Dependence of the weak-scale Dirac phase (left), BR($\mu \to e\gamma$) (middle) and BR($\tau \to \mu\gamma$) (right) on GUT-scale values of the Harrison-Scott parameters for benchmark point A with Yukawa unification parameter $R_{\nu u} = 1$. The contours for LFV branching ratios represent enhancement factors with respect to the point with $\delta = \pi/2$, $\{\phi, \chi\} = \{0, 0.294\}$ that is marked by the blue cross; all angles are in radians. The thick red lines are iso-θ_{13} contours for $\theta_{13} = 0.239$ [at the CHOOZ bound [93]; see Eq. (1.1)] and for the ultimate 90% C. L. reach of the Daya Bay experiment $\theta_{13} = 0.045$ [62]. The contours remain essentially unchanged for all other points with large mixing and for $R_{\nu u} = 3$.

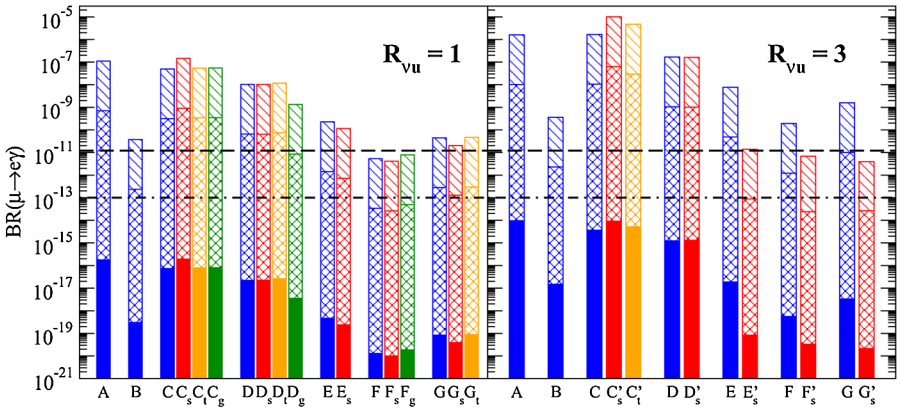

FIG. 3 (color online). Radiative LFV decay rates in the large mixing case for two values of $R_{\nu u}$ [c.f. Eqs. (2.4) and (2.7)]. The heights of the solid bars show rates for exact tribimaximal mixing $\chi = \phi = 0$ at the GUT scale. Diagonally hatched bars represent $\{\phi, \chi\} = \{0, 0.294\}$ yielding the maximum allowed θ_{13} and $\delta = \pi/2$. Cross-hatched bars represent $\{\phi, \chi\} = \{0, 0.022\}$, which has $\delta = \pi/2$ and $\theta_{13} \simeq 0.045$ that is the ultimate reach of the Daya Bay experiment. Dashed lines represent the current bound and dashed-dotted lines the projected sensitivity listed in Table II. The letters denote various benchmark points presented in Tables I, III, and IV. Points C through G have a RD above the WMAP bound. The corresponding WMAP-consistent points indicated by subscripts s, t and g are obtained by adjusting m_0, A_0 and $m_{1/2}$, respectively.

At point A in the $R_{\nu u} = 1$ case, BR($\mu \to e\gamma$) changes from 1.77×10^{-16} for $\phi = \chi = 0$, to 8.57×10^{-8} for $\{\phi, \chi\} = \{0, 0.294\}$; intermediate allowed ϕ and χ values produce rates between these values. For $\tau \to \mu\gamma$ and $\tau \to 3\mu$, the dependence on ϕ and χ parameters is reversed: larger ϕ and χ produce smaller rates. For example, at point A in the $R_{\nu u} = 1$ case, the $\tau \to \mu\gamma$ branching fraction is 2.09×10^{-7} for $\phi = \chi = 0$ and is 1.77×10^{-7} for $\{\phi, \chi\} = \{0, 0.294\}$. We see that $\tau \to \mu\gamma$ and $\tau \to 3\mu$ are excellent probes of LFV: the current experimental bound of $\tau \to \mu\gamma$ rules out the bulk region for all values of ϕ and χ.

In the stop-coannihilation region [27] the picture is radically different. A naive use of input parameters for point C gives a neutralino relic density $\Omega_{\tilde{Z}_1} h^2 = 0.34$, well above the WMAP bound. This is because $\tilde{t}_1$ is pushed to a higher mass causing stop-coannihilation to cease. To restore the stop-coannihilation mechanism and bring $\Omega_{\tilde{Z}_1} h^2$ down to the WMAP range, one can counteract the effect of $\mathbf{f}_\nu$ by adjusting SSB parameters. Adjusting the common scalar mass parameter m_0, with the rest of SSB parameters held fixed, can lower the stop mass back to the desired mass range leading to a new WMAP-consistent point that we denote[4] C_s with parameter values shown in

[4]Hereafter we use subscripts s, t, and g to denote points obtained from those in Table I by adjusting the value of one the model parameters: scalar mass m_0, trilinear coupling A_0 or gaugino mass $m_{1/2}$, respectively. Single and double primes are used to further distinguish modified points in the large mixing with $R_{\nu u} = 3$ and the small mixing with $R_{\nu u} = 1$ scenarios.

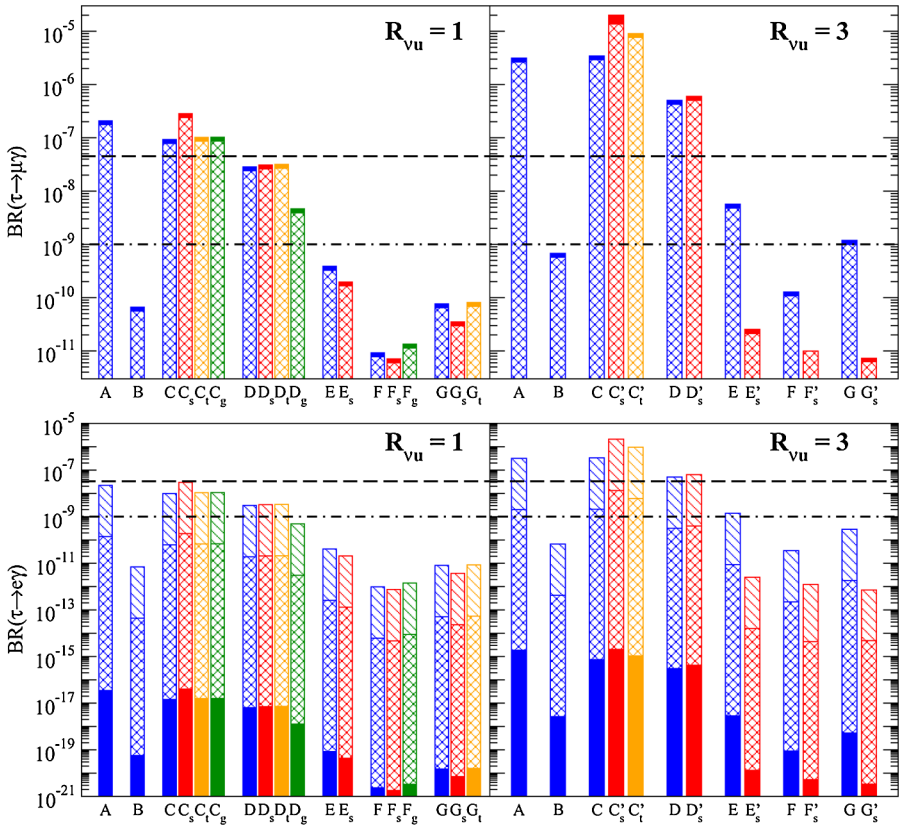

FIG. 4 (color online). Similar to Fig. 3 for τ radiative LFV decays. For $\tau \to \mu\gamma$, the $\{\phi, \chi\} = \{0, 0.022\}$ case is not shown as it produces rates very close to those for $\{\phi, \chi\} = \{0, 0.294\}$ (cross-hatched).

Table III. Increasing m_0 also makes sleptons lighter and increases their mixing, as can be seen from Eqs. (2.4) and (2.7), leading to a factor of $\sim$2.8 increase in LFV rates as compared to point C. The stop mass can also be lowered by dialing the trilinear A term, resulting in another modified point C_t. The rates increase with respect to values at point C by only about 10%. Alternatively, one can raise the $\tilde{Z}_1$ mass closer to that of the $\tilde{t}_1$ by adjusting the common gaugino mass parameter $m_{1/2}$ producing a correct RD at the point C_g. Since the required increase is small, rates again grow only by $\sim$10%.

In the A-funnel region [24,29], $\mathbf{f}_\nu$ pushes the mass of the CP-odd Higgs boson A up and away from the resonance, resulting in a larger RD of 0.144 for point D. This can be reduced by decreasing the scalar mass parameter (point D_s) or increasing the value of the trilinear A term (point D_t), which lower the A mass back to the resonance regime. In both cases, LFV rates increase by about 8%. Increasing the gaugino mass parameter can increase the $\tilde{Z}_1$ mass to the resonance value $m_{\tilde{Z}_1} = 0.5 m_A$. But the A mass also grows with $m_{1/2}$ although slower than the neutralino mass, so a large dialing is required, resulting in point D_g. This large change in $m_{1/2}$ increases the masses of the charginos in the loop resulting in about an order of magnitude drop in LFV rates.

In the lower part of the HB/FP region [28], at point E the RD is 2 orders of magnitude above the WMAP range. This is due to an increased value of μ from the $\mathbf{f}_\nu$ effect that can be counteracted by increasing m_0, resulting in new WMAP-allowed point E_s. The heavier sfermion spectrum causes LFV rates to decrease by about a factor of 2. Adjustment of the trilinear parameter can somewhat lower μ [6], but not enough to get back into the HB/FP regime. It would be possible to reduce the RD by lowering $m_{1/2}$ to 189 GeV, but at this value the chargino mass falls below the LEP2 bound of 103.5 GeV [64].

In the upper portion of the HB/FP region, the neutrino Yukawa couplings have an extremely large effect—the RD at point F becomes 12.3. Similarly to point E, the RD can be lowered by increasing the scalar mass parameter. In this part of the HB/FP region the chargino mass is sufficiently high that $m_{1/2}$ can be lowered without violating the LEP2 chargino bound, resulting in a WMAP-allowed value at point F_g. Since charginos become lighter with this adjustment, LFV rates increase by about 40%.

In the light Higgs resonance region [24,30], the neutrino Yukawa coupling also destabilizes the $\tilde{Z}_1$ annihilation mechanism producing too large a RD at point G. Although neither the $\tilde{Z}_1$ nor h masses are moved away from the desired regime $2m_{\tilde{Z}_1} = m_h$, the resonance mecha-

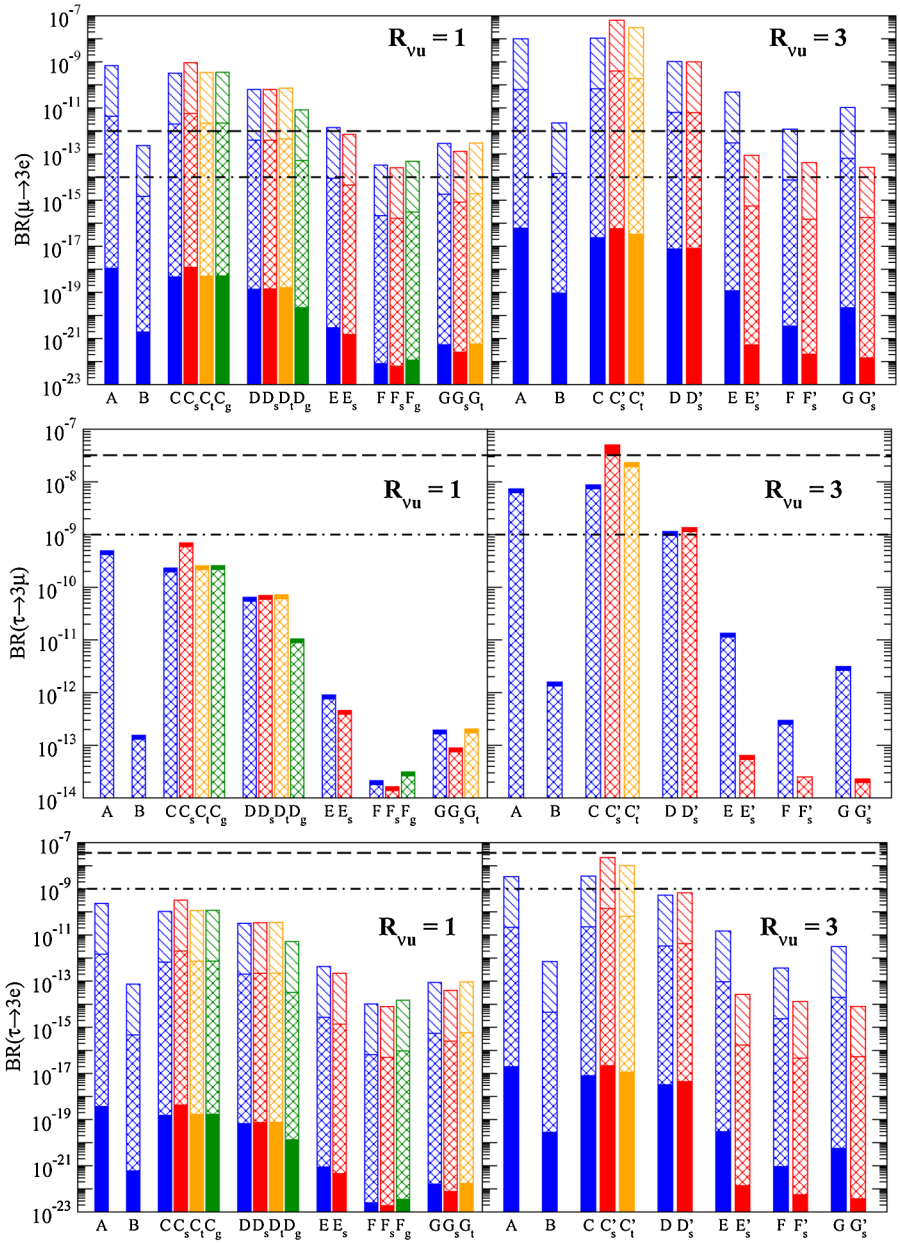

FIG. 5 (color online). Similar to Fig. 3 for trilepton LFV decays.

nism ceases to function because $\tilde{Z}_1$ becomes binolike and can no longer couple to the Higgs. The neutralino-Higgs coupling can be restored by lowering μ by increasing the scalar mass. This decreases LFV rates by about 20%. The desired value of the neutralino-Higgs coupling can also be achieved by adjustment of the trilinear parameter resulting in point G_t. In this case, the LFV rates increase only marginally compared to point G.

For $R_{\nu u} = 3$, we find that experimental limits (1.1) are satisfied for a GUT-scale Majorana mass matrix of the form

$$\mathbf{M}_N = \mathrm{diag}(4.5 \times 10^{-6}, 4.5 \times 10^{-5}, 1) \times 1.3 \times 10^{15}\ \mathrm{GeV}, \tag{3.3}$$

which we use in subsequent computations. This is a simple rescaling of Eq. (3.2) as expected from the seesaw formula. We have numerically verified that the dependence of the neutrino mixing parameters and LFV rates follow the same pattern shown in Fig. 2. Thus, rates on Figs. 3–6 are presented for the same choice of ϕ and χ discussed earlier.

As for $R_{\nu u} = 1$, the RD in points A and B remain unaffected by the presence of additional neutrino Yukawa couplings. However, the very large neutrino Yukawa generates large off-diagonal terms in the slepton mass matrix, as can be seen from Eq. (2.4), that boost LFV rates by more than an order of magnitude as compared to the $R_{\nu u} = 1$ case. Nevertheless, this is still not enough to rule out point B for the whole range of χ and ϕ values.

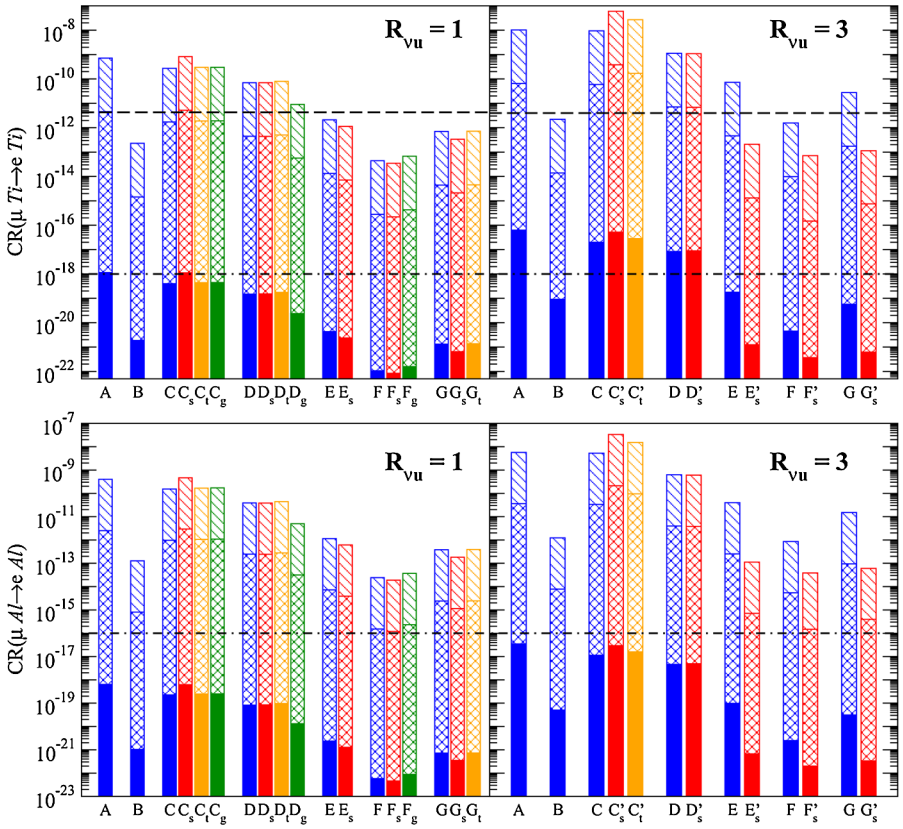

FIG. 6 (color online). Similar to Fig. 3 for LFV $\mu \rightarrow e$ conversion rates in titanium (upper frames) and aluminum (lower frames) targets.

At point C, the RD is too large: the $\tilde{t}_1$ mass is pushed further away from the $\tilde{Z}_1$ due to larger neutrino Yukawa effects. Thus. restoration of the stop-coannihilation mechanism requires larger adjustments of scalar mass and trilinear coupling parameters, leading to new WMAP-consistent points C_s' and C_t' listed in Table IV. Unlike the $R_{\nu u} = 1$ case, adjustment of $m_{1/2}$ cannot restore the stop-coannihilation: effects of $\mathbf{f}_\nu$ make $m_{\tilde{\tau}_1} < m_{\tilde{t}_1}$ and the RD is lowered to the WMAP range at $m_{1/2} = 725$ GeV by the stau-coannihilation mechanism. Increasing $m_{1/2}$ further makes $\tilde{\tau}_1$ the LSP before the stop-coannihilation regime can be reached.

In the A funnel, larger neutrino Yukawas push m_A away from the resonance resulting in $\Omega_{\tilde{Z}_1} h^2 = 0.33$ at point D. Lowering the scalar mass parameter can bring the A mass back into the resonance regime at point D_s'. The RD can also be lowered by either adjusting A_0 to -692 GeV or raising $m_{1/2}$ to 745 GeV. However, either of these bring the $\tilde{\tau}_1$ mass close to the $\tilde{Z}_1$ mass and activate the stau-coannihilation mechanism; further dialing of either parameter makes $\tilde{\tau}_1$ the LSP.

TABLE III. Modified benchmark points for mSUGRA seesaw in case of the large mixing with $R_{\nu u} = 1$ obtained from their counterparts in Table I by adjusting the parameter highlighted in boldface to produce the RD dictated byWMAP. All dimensionful parameters are in GeV. For all points $\mu > 0$ and $m_t = 171$ GeV.

Point	m_0	$m_{1/2}$	A_0	$\tan\beta$	Region
C_s	**94**	300	-1095	5	$\tilde{t}$-coan.
C_t	150	300	**-1120**	5	$\tilde{t}$-coan.
C_g	150	**294**	-1095	5	$\tilde{t}$-coan.
D_s	**440**	450	0	51	A-funnel
D_t	500	450	**150**	51	A-funnel
D_g	500	**724**	0	51	A-funnel
E_s	**1722**	300	0	10	HB/FP
F_s	**3607**	1000	0	10	HB/FP
F_g	3143	**806.5**	0	10	HB/FP
G_s	**2435**	130	-2000	10	h-funnel
G_t	2000	130	**-1680**	10	h-funnel

TABLE IV. Similar to Table III for the large mixing and $R_{\nu u} = 3$ case.

Point	m_0	$m_{1/2}$	A_0	$\tan\beta$	Region
C_s'	**96**	300	-1095	5	$\tilde{t}$-coan.
C_t'	150	300	**-1197**	5	$\tilde{t}$-coan.
D_s'	**355**	450	0	51	A-funnel
E_s'	**6061.5**	300	0	10	HB/FP
F_s'	**7434**	1000	0	10	HB/FP
G_s'	**6530**	130	-2000	10	h-funnel

In the HB/FP point E, μ is pushed by neutrino Yukawa coupling to very large values resulting in large RD, $\Omega_{\tilde{Z}_1}h^2 = 25$. To compensate, one needs to dial the scalar mass parameter to very high values (point E'_s). At such a large m_0, sleptons become very heavy causing LFV rates to drop by about 2 orders of magnitude. Consequently, rates for LFV muon decay and $\mu - e$ conversion fall below current limits for all χ and ϕ values. For this point, μ is so large that the HB/FP regime cannot be recovered by adjusting A_0 or $m_{1/2}$.

Similarly, for point F we get an extremely high relic density $\Omega_{\tilde{Z}_1}h^2 = 72$ that can be compensated by a very large scalar mass at point F'_s. The LFV rates are lowered by a factor of $\sim$15 so that muon LFV rates are below experimental bounds for all allowed mixing angles. As in the lower part of the HB/FP region, dialing A_0 or $m_{1/2}$ cannot bring $\Omega_{\tilde{Z}_1}h^2$ back in accord with WMAP.

In the h-resonance point G, μ is pushed so high that $\tilde{Z}_1$ becomes a pure bino state unable to couple to the Higgs boson. This can be compensated only by significantly increasing the scalar mass yielding a new WMAP-consistent point G'_s with LFV rates that are smaller by 2 orders of magnitude.

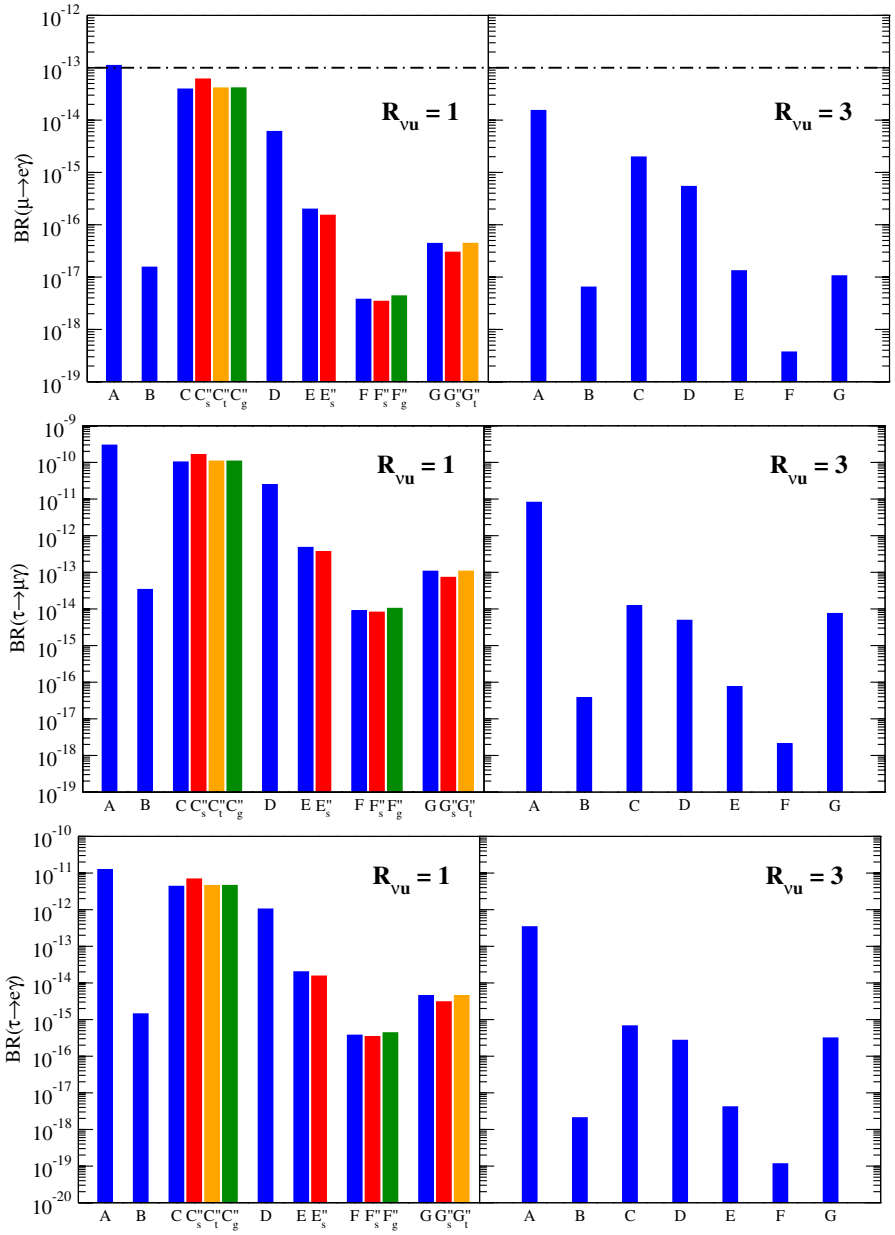

FIG. 7 (color online). Radiative LFV decay rates in the small mixing case for benchmark points presented in Tables I and V. All rates are below current experimental bounds. Dash-dotted lines represent the projected future sensitivity listed in Table II.

B. Small mixing

For the case of small mixing, we set $\mathbf{f}_\nu(M_{\rm GUT})$ according to Eq. (2.17) and choose the neutrino spectrum to be $m_{\nu_1} = 6\times10^{-4}$ eV, $m_{\nu_2} = 8\times10^{-3}$ eV, and $m_{\nu_3} = 5\times10^{-2}$ eV. Our choice for m_{ν_1} is constrained by the fact that we need $M_{N_1} \gg M_{\rm SUSY}$ for our approximation to remain valid. In this scenario LFV rates do not depend on neutrino mixing angles: Eq. (2.17) fixes the neutrino Yukawa matrix completely and perturbations of the structure of $\mathbf{M}_N$ do not produce significant changes in RGE evolution as can be seen from Eq. (2.4).

For $R_{\nu u} = 1$, full RGE evolution with our code yield the following eigenvalues of the Majorana mass matrix:

$$M_{N_1} \simeq 8\times10^4 \text{ GeV}, \qquad M_{N_2} \simeq 3.5\times10^9 \text{ GeV}, \qquad M_{N_3} \simeq 2.5\times10^{15} \text{ GeV}. \tag{3.4}$$

This would appear to be in conflict with thermal leptogenesis, which requires the lightest Majorana mass to be heavier than about 10^9 GeV [65]. Nevertheless, successful leptogenesis is possible through the decay of the next-to-lightest RHN [66]. Also notice that M_{N_3} is closer to $M_{\rm GUT}$ than it was in the case of large mixing. This, combined with small mixing in $\mathbf{f}_\nu$, lead to rates that are several orders of magnitude smaller, putting them all significantly below current experimental bounds, as shown in Figs. 7–9.

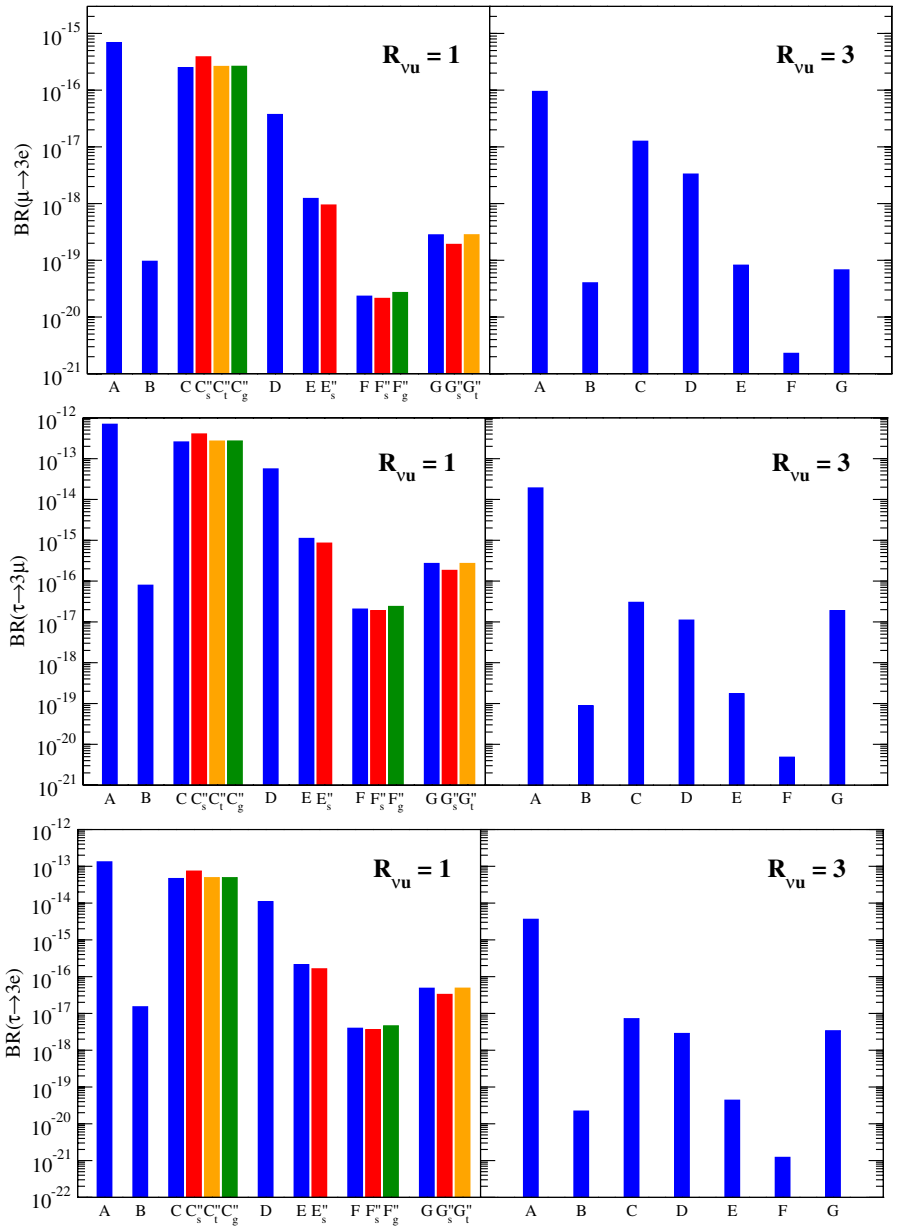

FIG. 8 (color online). Similar to Fig. 7 for trilepton LFV decays.

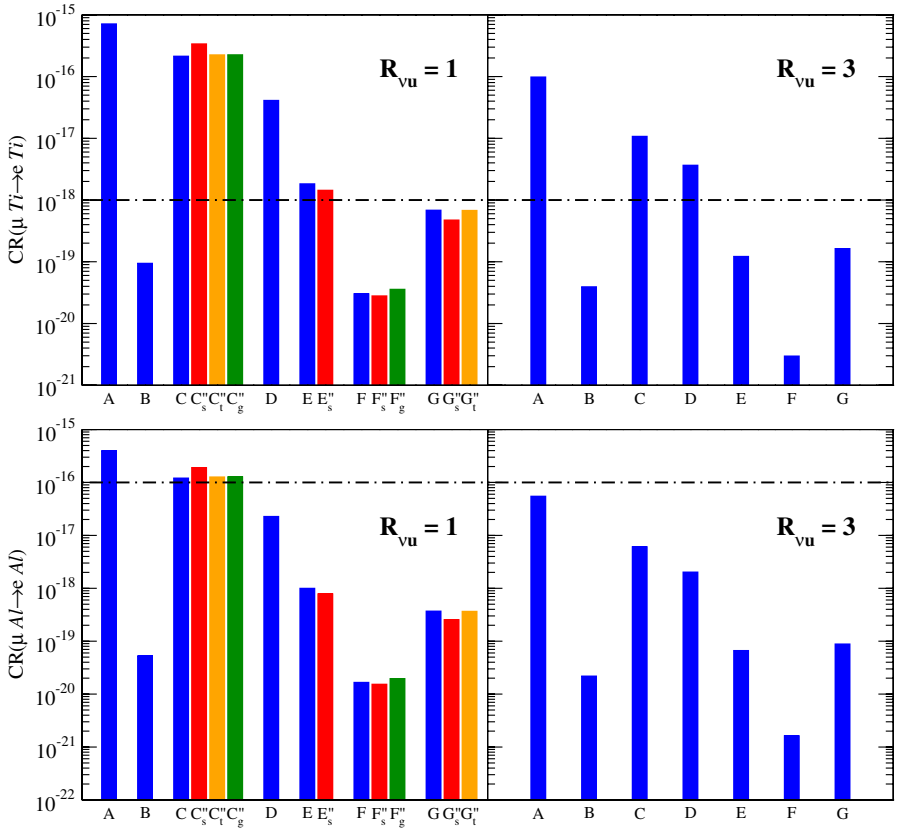

FIG. 9 (color online). Similar to Fig. 7 for LFV conversion rates in titanium (upper frames) and aluminum (lower frames) targets.

As discussed in Sec. III A, the use of mSUGRA values of points A and B still produces the correct RD. For example, at point A we have $\mathrm{BR}(\mu \to e\gamma) = 1.1 \times 10^{-13}$ that is barely above the reach of the future MEG experiment. In the A funnel, neutrino Yukawa couplings do affect the annihilation mechanism, but the effect is small and the RD remains within the WMAP range. For the other regions, adjustment of SSB parameters is necessary; the modified points are listed in Table V.

Even a decoupling scale as high as $M_{N_3} \sim 10^{15}$ GeV is enough to destabilize the stop-coannhilation mechanism, resulting in too large a RD for point C. Lowering the scalar mass parameter decreases the $\tilde{t}_1$ mass to the desired RD value at point C''_s, leading to a $\sim$50% increase in the LFV rates. The stop-coannihilation mechanism can also be restored by adjusting the trilinear A term (point C''_t) or the gaugino mass (point C''_g). In both cases, the LFV rates increase only slightly from those for point C. At all points $\mu \to e\gamma$ rates are slightly below the MEG reach, so this region will only be probed by $\mu \to e$ conversion experiments.

TABLE V. Similar to Table III for the small mixing and $R_{\nu u} = 1$ case.

Point	m_0	$m_{1/2}$	A_0	$\tan\beta$	Region
C''_s	**126**	300	−1095	5	$\tilde{t}$-coan.
C''_t	150	300	**−1106**	5	$\tilde{t}$-coan.
C''_g	150	**297**	−1095	5	$\tilde{t}$-coan.
E''_s	**1505**	300	0	10	HB/FP
F''_s	**3300**	1000	0	10	HB/FP
F''_g	3143	**943**	0	10	HB/FP
G''_s	**2205**	130	−2000	10	h-funnel
G''_t	2000	130	**−1895**	10	h-funnel

At point E, the RD is also too high. For the reasons discussed in Sec. III A, only adjustment of m_0 is possible, leading to consistency with WMAP for the values at point E''_s. Since the required shift is not as significant as in the large mixing case, the LFV rates drop only by $\sim$30%.

In the upper part of the HB/FP region at point D, the RD exceeds the WMAP value by 2 orders of magnitude. The desired Higgsino content of $\tilde{Z}_1$ can be restored by adjusting the scalar or gaugino mass parameters, giving points F''_s and F''_g. As a result, the LFV rates change by about 10% with respect to those at point D.

At point F, the Higgsino content of $\tilde{Z}_1$ is diminished by neutrino Yukawa RGE effects resulting in too high a RD. The h-resonance mechanism can be restored by adjusting the scalar mass (point G''_s) or the trilinear A term (point G''_t). These adjustments change the LFV rates approximately by a factor of 2 with respect to the prediction for point F.

For $R_{\nu u} = 3$, we find the eigenvalues of the Majorana mass matrix to be

$$M_{N_1} \simeq 7 \times 10^5 \text{ GeV}, \qquad M_{N_2} \simeq 3 \times 10^{10} \text{ GeV}, \qquad M_{N_3} \simeq 2.2 \times 10^{16} \text{ GeV}. \tag{3.5}$$

The heaviest Majorana mass value is very close to $M_{\rm GUT} \simeq 2.3 \times 10^{16}$ GeV. Because of this, the effect of $\mathbf{f}_\nu$ on RD is negligible and WMAP-consistent values are obtained for the mSUGRA points in Table I. From the resultant LFV rates in Figs. 7–9, we see that the larger neutrino Yukawa coupling produces LFV rates that are smaller by almost an order of magnitude. This is opposite to what we saw in the large mixing scenarios where $R_{\nu u} = 3$ rates were more than an order of magnitude greater that their $R_{\nu u} = 1$ cousins. This is also a direct consequence of the proximity of M_{N_3} to $M_{\rm GUT}$: the largest neutrino Yukawa decouples almost immediately and off-diagonal elements in the slepton doublet matrix are generated by the much smaller Yukawas of the first and second generations.

IV. DISCUSSION

We perfomed a detailed study of the LFV rates in the RD-allowed benchmark points, and demonstrated that the interconnection between the neutrino sector and neutralino dark matter is very important for predictions of LFV rates. Proper consideration of these effects change LFV rates by factor of a few to up to 2 orders of magnitude. We emphasize that although we used $SO(10)$ models to set the structure of the neutrino Yukawa matrix at the GUT scale, our results are generic; they hold in any type-I SUSY-seesaw scenario with large neutrino Yukawa couplings.

The results in Sec. III imply the following about models with universal (or mSUGRA-like) SSB boundary conditions stipulated at the GUT scale:

(i) The small mixing scenario is completely consistent with present experimental bounds on LFV. Upcoming $\mu \to e\gamma$ experiments will probe only a very small corner of parameter space where both m_0 and $m_{1/2}$ are small and $R_{\nu u} = 1$. Future $\mu \to e$ conversion experiments, although suppressed by a factor $\sim Z\alpha/\pi$ with respect to $\mu \to e\gamma$, have better prospects due to the very well defined experimental signal. The PRIME experiment will be able to probe the entire bulk and stop-coannihilation regions as well as a significant portion of the A-funnel region, while the Mu2e experiment will only be able to probe the bulk and stop-coannihilation regions for $R_{\nu u} = 1$.

(ii) Contrary to naive expectations, in the small mixing case, order of magnitude *smaller* LFV rates are expected for $R_{\nu u} = 3$ than for $R_{\nu u} = 1$. Such small rates will only be probed by the PRIME $\mu \to e$ conversion experiment with a Ti target.

(iii) Future $\mu \to e\gamma$ measurements will not rule out large mixing scenarios for any values of ϕ and χ in the mixing matrix of Eq. (2.15) because of the high sensitivity of this channel to θ_{13}. On the other hand, if θ_{13} is close to the CHOOZ bound, only the HB/FP and h-funnel regions are consistent with current limits.

(iv) The $\tau \to \mu\gamma$ channel is an excellent probe as it is not sensitive to θ_{13}. Current experimental limits exclude the bulk region and the stop-coannihilation regions. For large $R_{\nu u}$, part of the A-funnel region is also excluded. Future experiments at super flavor factories [37] should be able to probe the A-funnel region almost entirely.

(v) Trilepton decays are weaker probes due to a factor $\sim\alpha$ suppression of the rates as compared to the two body modes. Nevertheless, current data rule out θ_{13} close to the CHOOZ bound for some regions of SUSY parameter space.

(vi) $\mu \to e$ conversion in nuclei is the best probe of LFV. Future experiments will have sensitivity to almost the entire parameter space. In the large mixing case, $\mu \to e$ conversion is highly complementary to collider searches: it can probe large parts of the HB/FP region, which can not be probed at the LHC.

The upcoming Daya Bay and Double Chooz experiments will soon be able to probe θ_{13} independently of the Dirac phase down to $\sin^2\theta_{13} = 0.002$. A signal of nonzero θ_{13} will significantly reduce uncertainties in the predictions of LFV rates if the observed neutrino mixing arises dominantly from $\mathbf{f}_\nu$ as in the large mixing case. The θ_{13}-dependent LFV rates will be within about 2 orders of magnitude of the maximum values shown in Figs. 3–6 thus further constraining model parameter space with current LFV data. For instance, the current $\mu \to e\gamma$ bound rules out a significant portion of the A funnel for the case of large mixing and either value of $R_{\nu u}$. With future $\mu \to e\gamma$ measurements we will be able to tell if the type-I SUSY-seesaw can be realized in the stau-coannihilation region with large $\mathbf{f}_\nu$ mixing regardless of $R_{\nu u}$; see point B in Fig. 3.

If the LHC finds a signal of SUSY, then GUTs become very appealing. One might be able to combine the knowledge of the sparticle spectrum from the LHC with results from LFV experiments to determine the value of $R_{\nu u}$ and/or get some information about the mixing pattern in the neutrino Yukawa. For example, if SUSY is found to be realized in the bulk region (point A), then a type-I SUSY-seesaw can only exist if the mixing in $\mathbf{f}_\nu$ is small. Then measurements from the PRIME experiment could be used to identify $R_{\nu u}$. The situation becomes even more favorable if θ_{13} is known. For example, if SUSY is found to be consistent with the A-funnel region, then with the value of θ_{13} in hand, PRIME measurements will be able to test if the type-I SUSY-seesaw is operative for all mixing patterns and $R_{\nu u}$ values.

V. CONCLUSIONS

In previous work [32] we demonstrated that large neutrino Yukawa couplings can significantly affect the neutralino relic density. This effect can be counteracted by the adjustment of SSB parameters, with concomitant changes in the low-energy phenomenology. In this work, we studied LFV processes in the type-I SUSY-seesaw properly taking into account neutrino Yukawa effects on the neutralino RD. For simplicity, we considered a scenario with flavor-blind universal (or mSUGRA-like) boundary conditions defined at the GUT scale. In the neutrino sector we utilized the "top-down" approach in which neutrino Yukawa and Majorana mass matrices are inputs at $M_{\rm GUT}$. We considered two cases for the neutrino-up-quark unification parameter $R_{\nu u}$ [see Eq. (2.13)], which are inspired by $SO(10)$ models. For each scenario we examined two extreme cases for the mixing in the neutrino Yukawa matrix. We found that the common practice of using WMAP-allowed points of mSUGRA in models with RHNs overestimates the LFV rates in most regions of parameter space.

In the $R_{\nu u} = 1$ case we found that the neutrino-neutralino interplay can result in significant changes in LFV predictions. The rates can change by a factor of up to 5 in the WMAP-allowed regions as compared to naive estimates. Effects are most prominent in regions with a large scalar mass parameter m_0 such as HP/FP and h-funnel regions. If the mixing in the neutrino Yukawa matrix is small, then all LFV rates are below current experimental bounds. In the future, this case can be probed to some extent by the MEG experiment and by the PRIME and Mu2e conversion experiments.

The case of very large unification parameter $R_{\nu u} = 3$, contrary to common lore, is not ruled out by current bounds on LFV processes even if the mixing in the neutrino Yukawa matrix is large. In the large mixing case a proper treatment of the neutralino-neutrino interplay leads to LFV rates that are smaller by about 2 orders of magnitude than naively expected. As result, many rates fall below current limits. Surprisingly, we found that if mixing in the neutrino Yukawa matrix is small, then for $R_{\nu u} = 3$, the LFV rates are an order of magnitude smaller than for $R_{\nu u} = 1$. If this scenario is realized, then only the future PRIME experiment will have sensitivity to some regions of the parameter space.

ACKNOWLEDGMENTS

We thank A. Belyaev, S. Blanchet, A. Box, M. Malinsky, H. Päs, and X. Tata for discussions and useful input, and A. Box and X. Tata for forwarding us the unpublished erratum of Ref. [80]. V. B. and D. M. thank the Aspen Center for Physics for hospitality. This work was supported by the DoE under Grant Nos. DE-FG02-95ER40896 and DE-FG02-04ER41308, by the NSF under Grant No. PHY-0544278, and by the Wisconsin Alumni Research Foundation.

APPENDIX A: NOTATION AND CONVENTIONS

Here, we briefly list the most relevant equations to establish our formalism; we follow the notation and conventions of Ref. [5].

The MSSM superpotential has the form

$$\hat{f} = \mu \hat{H}_u^a \hat{H}_{da} + \sum_{i,j=1,3} [(\mathbf{f}_u)_{ij} \epsilon_{ab} \hat{Q}_i^a \hat{H}_u^b \hat{U}_j^c + (\mathbf{f}_d)_{ij} \hat{Q}_i^a \hat{H}_{da} \hat{D}_j^c + (\mathbf{f}_e)_{ij} \hat{L}_i^a \hat{H}_{da} \hat{E}_j^c], \tag{A1}$$

where a, b are $SU(2)_L$ doublet indices, i, j are generation indices, ϵ_{ab} is the totally antisymmetric tensor with $\epsilon_{12} = 1$ and the superscript c denotes charge conjugation.

The soft SUSY breaking part of the Lagrangian is

$$\begin{aligned}\mathcal{L}_{\rm soft}^{\rm MSSM} = & -[\tilde{Q}_i^\dagger (\mathbf{m}_{\mathbf{Q}}^2)_{ij} \tilde{Q}_j + \tilde{d}_{Ri}^\dagger (\mathbf{m}_{\mathbf{D}}^2)_{ij} \tilde{d}_{Rj} + \tilde{u}_{Ri}^\dagger (\mathbf{m}_{\mathbf{U}}^2)_{ij} \tilde{u}_{Rj} \\ & + \tilde{L}_i^\dagger (\mathbf{m}_{\mathbf{L}}^2)_{ij} \tilde{L}_j + \tilde{e}_{Ri}^\dagger (\mathbf{m}_{\mathbf{E}}^2)_{ij} \tilde{e}_{Rj} + m_{H_u}^2 |H_u|^2 \\ & + m_{H_d}^2 |H_d|^2] - \frac{1}{2}[M_1 \bar{\lambda}_0 \lambda_0 + M_2 \bar{\lambda}_A \lambda_A \\ & + M_3 \bar{\tilde{g}}_B \tilde{g}_B] + [(\mathbf{a}_{\mathbf{u}})_{ij} \epsilon_{ab} \tilde{Q}_i^a H_u^b \tilde{u}_{Rj}^\dagger \\ & + (\mathbf{a}_{\mathbf{d}})_{ij} \tilde{Q}_i^a H_{da} \tilde{d}_{Rj}^\dagger + (\mathbf{a}_{\mathbf{e}})_{ij} \tilde{L}_i^a H_{da} \tilde{e}_{Rj}^\dagger \\ & + \text{H.c.}] + [b H_u^a H_{da} + \text{H.c.}].\end{aligned} \tag{A2}$$

The gaugino fields $\tilde{g}_B (B = 1 \ldots 8)$, $\lambda_A (A = 1 \ldots 3)$ and λ_0 transform according to the adjoint representations of $SU(3)_c$, $SU(2)_L$, and $U(1)_Y$, respectively.

We use the RL convention for the fermion mass term, $\mathcal{L}_{\rm mass} = -(\bar{\psi}_R^i m_{ij} \psi_L^j + \text{H.c.})$, in which physical (real and diagonal) mass matrices read

$$\boldsymbol{m}_u = v_u \mathbf{V}_{\mathbf{u_R}} \mathbf{f}_u^T \mathbf{V}_{\mathbf{u_L}}^\dagger, \qquad \boldsymbol{m}_d = v_d \mathbf{V}_{\mathbf{d_R}} \mathbf{f}_d^T \mathbf{V}_{\mathbf{d_L}}^\dagger, \qquad \boldsymbol{m}_e = v_d \mathbf{V}_{\mathbf{e_R}} \mathbf{f}_e^T \mathbf{V}_{\mathbf{e_L}}^\dagger, \tag{A3}$$

where v_u, v_d are up- and down-Higgs VEVs with $v = \sqrt{v_u^2 + v_d^2} \simeq 174$ GeV. The unitary rotation matrices $\mathbf{V}_\bullet$ transform gauge eigenstates (unprimed) to mass eigenstates (primed) as follows:

$$\begin{aligned} u'_{Li} &= (\mathbf{V}_{\mathbf{u_L}})_{ij} u_{Lj}, & u'_{Ri} &= (\mathbf{V}_{\mathbf{u_R}})_{ij} u_{Rj}, \\ d'_{Li} &= (\mathbf{V}_{\mathbf{d_L}})_{ij} d_{Lj}, & d'_{Ri} &= (\mathbf{V}_{\mathbf{d_R}})_{ij} d_{Rj}, \\ e'_{Li} &= (\mathbf{V}_{\mathbf{e_L}})_{ij} e_{Lj}, & e'_{Ri} &= (\mathbf{V}_{\mathbf{e_R}})_{ij} e_{Rj}. \end{aligned} \tag{A4}$$

The CKM matrix [67] is $\mathbf{V}_{\rm CKM} = \mathbf{V}_{\mathbf{u_L}} \mathbf{V}_{\mathbf{d_L}}^\dagger$. Because of different matrix diagonalization conventions, our rotation matrices $\mathbf{V}_\bullet$ are Hermitian conjugates of those in Ref. [68,69].

We work in the super-CKM (SCKM) basis [70] where gluino vertices remain flavor diagonal. Here, the diagonalization of sfermion mass matrices proceeds in two steps. First, the squarks and sleptons are rotated "in parallel" to their fermionic superpartners

$$\begin{aligned}
\tilde{u}'_{Li} &= (\mathbf{V}_{\mathbf{u_L}})_{ij}\tilde{u}_{Lj}, & \tilde{u}'_{Ri} &= (\mathbf{V}_{\mathbf{u_R}})_{ij}\tilde{u}_{Rj},\\
\tilde{d}'_{Li} &= (\mathbf{V}_{\mathbf{d_L}})_{ij}\tilde{d}_{Lj}, & \tilde{d}'_{Ri} &= (\mathbf{V}_{\mathbf{d_R}})_{ij}\tilde{d}_{Rj},\\
\tilde{e}'_{Li} &= (\mathbf{V}_{\mathbf{e_L}})_{ij}\tilde{e}_{Lj}, & \tilde{e}'_{Ri} &= (\mathbf{V}_{\mathbf{e_R}})_{ij}\tilde{e}_{Rj},\\
\tilde{\nu}'_{Li} &= (\mathbf{V}_{\mathbf{e_L}})_{ij}\tilde{\nu}_{Lj},
\end{aligned} \tag{A5}$$

where the SCKM scalar fields (primed) form supermultiplets with the corresponding fermion mass eigenstates, i.e., SCKM basis preserves the superfield structure after diagonalization of fermions. Next, 6×6 sfermion mass-squared matrices in the SCKM basis are constructed:

$$\begin{aligned}
\mathcal{M}^2_{\tilde{u}} &= \begin{pmatrix} \mathbf{M}^2_{\tilde{u}LL} + \boldsymbol{m}_u^2 + D(\tilde{u}_L)\mathbb{1} & -\mathbf{M}^2_{\tilde{u}LR} + \mu\cot\beta \boldsymbol{m}_u \\ -\mathbf{M}^{2\dagger}_{\tilde{u}LR} + \mu^*\cot\beta \boldsymbol{m}_u & \mathbf{M}^2_{\tilde{u}RR} + \boldsymbol{m}_u^2 + D(\tilde{u}_R)\mathbb{1} \end{pmatrix},\\
\mathcal{M}^2_{\tilde{d}} &= \begin{pmatrix} \mathbf{M}^2_{\tilde{d}LL} + \boldsymbol{m}_d^2 + D(\tilde{d}_L)\mathbb{1} & -\mathbf{M}^2_{\tilde{d}LR} + \mu\tan\beta \boldsymbol{m}_d \\ -\mathbf{M}^{2\dagger}_{\tilde{d}LR} + \mu^*\tan\beta \boldsymbol{m}_d & \mathbf{M}^2_{\tilde{d}RR} + \boldsymbol{m}_d^2 + D(\tilde{d}_R)\mathbb{1} \end{pmatrix},\\
\mathcal{M}^2_{\tilde{e}} &= \begin{pmatrix} \mathbf{M}^2_{\tilde{e}LL} + \boldsymbol{m}_e^2 + D(\tilde{e}_L)\mathbb{1} & -\mathbf{M}^2_{\tilde{e}LR} + \mu\tan\beta \boldsymbol{m}_e \\ -\mathbf{M}^{2\dagger}_{\tilde{e}LR} + \mu^*\tan\beta \boldsymbol{m}_e & \mathbf{M}^2_{\tilde{e}RR} + \boldsymbol{m}_e^2 + D(\tilde{d}_R)\mathbb{1} \end{pmatrix},
\end{aligned} \tag{A6}$$

where $D(\tilde{f})$ are the hypercharge D-term contributions to the corresponding sfermions, $\mathbb{1}$ is the 3×3 unit matrix, $\boldsymbol{m}_f$ are the diagonal fermion mass matrices of Eq. (A3), and the flavor-changing entries are contained in rotated SSB matrices,

$$\begin{aligned}
\mathbf{M}^2_{\tilde{u}LL} &= \mathbf{V}_{\mathbf{u_L}}\mathbf{m}^2_{\mathbf{Q}}\mathbf{V}^\dagger_{\mathbf{u_L}}, & \mathbf{M}^2_{\tilde{u}RR} &= \mathbf{V}_{\mathbf{u_R}}\mathbf{m}^2_{\mathbf{U}}\mathbf{V}^\dagger_{\mathbf{u_R}},\\
\mathbf{M}^2_{\tilde{u}LR} &= \mathbf{V}_{\mathbf{u_L}}\mathbf{a}^*_{\mathbf{u}}\mathbf{V}^\dagger_{\mathbf{u_R}}, & \mathbf{M}^2_{\tilde{d}LL} &= \mathbf{V}_{\mathbf{d_L}}\mathbf{m}^2_{\mathbf{Q}}\mathbf{V}^\dagger_{\mathbf{d_L}},\\
\mathbf{M}^2_{\tilde{d}RR} &= \mathbf{V}_{\mathbf{d_R}}\mathbf{m}^2_{\mathbf{D}}\mathbf{V}^\dagger_{\mathbf{d_R}}, & \mathbf{M}^2_{\tilde{d}LR} &= \mathbf{V}_{\mathbf{d_L}}\mathbf{a}^*_{\mathbf{d}}\mathbf{V}^\dagger_{\mathbf{d_R}},\\
\mathbf{M}^2_{\tilde{e}LL} &= \mathbf{V}_{\mathbf{e_L}}\mathbf{m}^2_{\mathbf{L}}\mathbf{V}^\dagger_{\mathbf{e_L}}, & \mathbf{M}^2_{\tilde{e}RR} &= \mathbf{V}_{\mathbf{e_R}}\mathbf{m}^2_{\mathbf{E}}\mathbf{V}^\dagger_{\mathbf{e_R}},\\
\mathbf{M}^2_{\tilde{e}LR} &= \mathbf{V}_{\mathbf{e_L}}\mathbf{a}^*_{\mathbf{e}}\mathbf{V}^\dagger_{\mathbf{e_R}}.
\end{aligned} \tag{A7}$$

Note that the squark doublet mass-squared SSB matrix $\mathbf{m}^2_{\mathbf{Q}}$ is rotated differently for $\mathcal{M}^2_{\tilde{u}}$ and $\mathcal{M}^2_{\tilde{d}}$. Because of the absence of right-handed neutrino states in the MSSM, the sneutrino mass-squared matrix is a 3×3 matrix of the form

$$\mathcal{M}^2_{\tilde{\nu}} = \mathbf{V}_{\mathbf{e_L}}\mathbf{m}^2_{\mathbf{L}}\mathbf{V}^\dagger_{\mathbf{e_L}} + D(\tilde{\nu}_L)\mathbb{1}. \tag{A8}$$

Finally, the mass-squared matrices (A6) and (A8) are diagonalized to obtain sfermion mass eigenstates. These mass eigenstates are labeled in ascending mass order.

To incorporate neutrino masses, we employ the type-I seesaw mechanism, where the MSSM is extended by three gauge singlet superfields $\hat{N}^c_i$ each of whose fermionic component is the left-handed antineutrino and scalar component is $\tilde{\nu}^\dagger_{Ri}$. The extended superpotential has the form shown in Eq. (2.1). The neutrino Yukawa and Majorana mass matrices are diagonalized in analogy with Eq. (A3) by unitary matrices $\mathbf{V}_{\nu_\mathbf{L}}$, $\mathbf{V}_{\nu_\mathbf{R}}$ and $\mathbf{V}_\mathbf{N}$ according to

$$\begin{aligned}
\boldsymbol{m}_D &= \upsilon_u \mathbf{V}_{\nu_\mathbf{R}}\mathbf{f}^T_\nu\mathbf{V}^\dagger_{\nu_\mathbf{L}},\\
\mathbf{V}_\mathbf{N}\mathbf{M}_\mathbf{N}\mathbf{V}^T_\mathbf{N} &= \mathrm{diag}(M_{N_1}, M_{N_2}, M_{N_3}),
\end{aligned} \tag{A9}$$

where $\boldsymbol{m}_D$ is the Dirac neutrino mass matrix. *A priori* the eigenvalues M_{N_i} are arbitrary, but the observed large difference between neutrino and charged lepton masses strongly suggests that the scale of Majorana masses $M_{\mathrm{Maj}} \equiv \max(M_{N_3})$ is much higher than the weak scale. Additional soft SUSY breaking terms should also be included so that the Lagrangian becomes

$$\begin{aligned}
\mathcal{L}_{\mathrm{soft}} = \mathcal{L}^{\mathrm{MSSM}}_{\mathrm{soft}} &- \tilde{\nu}^\dagger_{Ri}(\mathbf{m}^2_{\tilde{\nu}_R})_{ij}\tilde{\nu}_{Rj} + \Big[(\mathbf{a}_\nu)_{ij}\epsilon_{ab}\tilde{L}^a_i\tilde{H}^b_u\tilde{\nu}^\dagger_{Rj}\\
&+ \tfrac{1}{2}(\mathbf{b}_\nu)_{ij}\tilde{\nu}_{Ri}\tilde{\nu}_{Rj} + \mathrm{H.c.}\Big].
\end{aligned} \tag{A10}$$

The eigenvalues of matrices $\mathbf{a}_\nu$ and $\mathbf{b}_\nu$ and the square roots of the eigenvalues of $\mathbf{m}^2_{\tilde{\nu}_R}$, are assumed to be of the order of the weak scale M_{weak}.

Above the scale M_{Maj}, the mass matrix for left-handed neutrinos is given by Eq. (2.2). This is the minimal or type-I seesaw mechanism [3]. At low energies all RHNs decouple and the theory is governed by the effective superpotential,

$$\hat{f}_{\mathrm{eff}} = \hat{f}_{\mathrm{MSSM}} + \tfrac{1}{2}\kappa_{ij}\epsilon_{ab}\hat{L}^a_i\hat{H}^b_u\epsilon_{df}\hat{L}^d_j\hat{H}^f_u. \tag{A11}$$

Here, κ is a 3×3 complex symmetric coupling matrix that breaks lepton number explicitly, and is determined by matching conditions at RHN thresholds,

$$(\kappa)_{ij}|_{M^-_{N_k}} = (\kappa)_{ij}|_{M^+_{N_k}} + (\mathbf{f}_\nu)_{ik}\frac{1}{M_{N_k}}(\mathbf{f}^T_\nu)_{ik}|_{M^+_{N_k}}, \tag{A12}$$

where $M^+_{N_k}(M^-_{N_k})$ denotes the value as the scale of decoupling of the k-th generation RHN M_{N_k} is approached from above (below).

After electroweak symmetry breaking, the Majorana mass matrix for light left-handed neutrinos is simply $\mathcal{M}_\nu = -\kappa\upsilon_u^2$. The symmetric 3×3 matrix $\mathcal{M}_\nu$ can be diagonalized as

$$\mathbf{U}_\nu\mathcal{M}_\nu\mathbf{U}^T_\nu = \boldsymbol{m}_\nu, \tag{A13}$$

where $\mathbf{U}_\nu$ is a unitary matrix and $\boldsymbol{m}_\nu$ is a diagonal matrix of the physical neutrino masses m_1, m_2, and m_3. In labeling the (real non-negative) mass eigenstates we follow the usual convention that 1 and 2 denote states with the smallest mass-squared difference and $m_1 < m_2$. The MNS mixing matrix of physical neutrinos [71] then has the form $\mathbf{V}_{\mathrm{MNS}} = \mathbf{V}_{\mathbf{e_L}}\mathbf{U}^\dagger_\nu$. Note that as a consequence of the seesaw mechanism, $\mathbf{U}_\nu$ is in general different from the neutrino Yukawa diagonalization matrix $\mathbf{V}_{\nu_\mathbf{L}}$ defined in Eq. (A9).

The MNS matrix can be parametrized as

$$\mathbf{V}_{\rm MNS} = \begin{pmatrix} c_{12}c_{13} & s_{12}c_{13} & s_{13}e^{-i\delta} \\ -c_{23}s_{12} - s_{23}s_{13}c_{12}e^{i\delta} & c_{23}c_{12} - s_{23}s_{13}s_{12}e^{i\delta} & s_{23}c_{13} \\ s_{23}s_{12} - c_{23}s_{13}c_{12}e^{i\delta} & -s_{23}c_{12} - c_{23}s_{13}s_{12}e^{i\delta} & c_{23}c_{13} \end{pmatrix} \times \mathrm{diag}(e^{i(\phi_1/2)}, e^{i(\phi_2/2)}, 1), \tag{A14}$$

with $s_{ij} = \sin\theta_{ij}$ and $c_{ij} = \cos\theta_{ij}$, θ_{ij} are mixing angles and the Dirac and Majorana CP-violating phases are δ, $\phi_{1,2} \in [0, 2\pi]$, respectively.

The addition of the $\hat{N}_i^c$ superfields also leads to an expansion of the sneutrino mass-squared matrix: it is now a 12×12 matrix, so that the relevant part of Lagrangian is

$$\mathcal{L} \ni -\frac{1}{2}\tilde{n}^\dagger \begin{pmatrix} \mathcal{M}^2_{L^\dagger L} & 0 & \mathcal{M}^2_{L^\dagger R} & v_u \mathbf{f}^*_\nu \mathbf{M}^T_{\mathbf{N}} \\ 0 & (\mathcal{M}^2_{L^\dagger L})^T & v_u \mathbf{f}_\nu \mathbf{M}^\dagger_{\mathbf{N}} & (\mathcal{M}^2_{L^\dagger R})^* \\ (\mathcal{M}^2_{L^\dagger R})^\dagger & v_u \mathbf{M}_{\mathbf{N}} \mathbf{f}^\dagger_\nu & \mathcal{M}^2_{R^\dagger R} & -\mathbf{b}^\dagger_\nu \\ v_u \mathbf{M}^*_{\mathbf{N}} \mathbf{f}^T_\nu & (\mathcal{M}^2_{L^\dagger R})^T & -\mathbf{b}_\nu & (\mathcal{M}^2_{R^\dagger R})^T \end{pmatrix} \tilde{n}, \tag{A15}$$

where $\tilde{n}^T \equiv (\tilde{\nu}_L^T, \tilde{\nu}_L^\dagger, \tilde{\nu}_R^T, \tilde{\nu}_R^\dagger)$, 0 is the 3×3 null matrix and

$$\begin{aligned} \mathcal{M}^2_{L^\dagger L} &= \mathbf{m}^2_{\mathbf{L}} + v_u^2 \mathbf{f}^*_\nu \mathbf{f}^T_\nu + D(\tilde{\nu}_L)\mathbb{1}, \\ \mathcal{M}^2_{R^\dagger R} &= \mathbf{m}^2_{\tilde{\nu}_R} + v_u^2 \mathbf{f}^T_\nu \mathbf{f}^*_\nu + \mathbf{M}_{\mathbf{N}} \mathbf{M}^\dagger_{\mathbf{N}}, \\ \mathcal{M}^2_{L^\dagger R} &= -v_u \mathbf{a}^*_\nu + \mu v_d \mathbf{f}^*_\nu. \end{aligned} \tag{A16}$$

From this structure we see that there is sneutrino-antisneutrino mixing for right-handed states introduced by $\mathbf{b}_\nu$ with no corresponding terms in the left-handed sector. The Majorana mass matrix $\mathbf{M}_{\mathbf{N}}$ contributes to the mass of the right-handed states and also results in the mixing of right-handed antisneutrino states with left-handed sneutrinos. Since $\mathbf{M}_{\mathbf{N}}$ eigenvalues are much larger than the rest of the SSB parameters the matrix exhibits a seesaw-type behavior, similar to the one for neutrinos: the 6×6 L-L block is of $\mathcal{O}(M^2_{\rm weak})$, while R-L blocks are of $\mathcal{O}(M_{\rm weak} M_{\rm Maj})$ and the R-R block is $\mathcal{O}(M^2_{\rm Maj})$. Therefore, the right-handed sneutrinos decouple and the phenomenologically relevant left-handed sneutrinos have a mass-squared matrix of the familiar MSSM form (A8).

APPENDIX B: DESCRIPTION OF ISAJET-M

In this section we describe the algorithm used to perform the calculation. Our code, named ISAJET-M, is ISAJET 7.78 [55] modified to evolve all couplings and SSB parameters, including the neutrino sector, in full matrix form at the 2-loop level. The following standard model parameters are used as inputs: fermion masses, the Z-boson pole mass M_Z, the fine structure constant $\alpha^{\overline{\rm MS}}(M_Z)$, the strong coupling constant $\alpha_s^{\overline{\rm MS}}(M_Z)$ and CKM angles in the "standard parametrization"; see Table VI.

In the first step $\alpha^{\overline{\rm MS}}$ and $\alpha_s^{\overline{\rm MS}}$ are evolved from $Q = M_Z$ down to $Q = 2$ GeV using 2-loop QCD $\times$ QED RGEs with the additional 3rd QCD loop [73,74]. We use step-function decoupling of fermions at the scale of their running mass and include finite threshold corrections at 2 loops according to Ref. [75]. Then we compute the running lepton masses $m_l^{\overline{\rm MS}}(2\ {\rm GeV})$ from their pole masses m_l using the 1-loop expression in the $\overline{\rm MS}$ scheme [73]:

$$m_l^{\overline{\rm MS}}(Q) = m_l\left[1 - \frac{\alpha^{\overline{\rm MS}}(Q)}{\pi}\left(1 + \frac{3}{4}\ln\frac{Q^2}{m_l^2}\right)\right]. \tag{B1}$$

Next, the two gauge couplings and all SM fermion masses (except for the top mass) are run up to M_Z. Here, fermion masses are converted from $\overline{\rm MS}$ to $\overline{\rm DR}$ scheme using formulae given in Refs. [76,77]:

$$\begin{aligned} m_b^{\overline{\rm DR}}(M_Z) &= m_b^{\overline{\rm MS}}(M_Z) \\ &\quad \times \left(1 - \frac{\alpha_s}{3\pi} - \frac{29\alpha_s^2}{72\pi^2} + \frac{3g_2^2}{128\pi^2} + \frac{13g_1^2}{1920\pi^2}\right)_{\overline{\rm MS}}, \\ m_c^{\overline{\rm DR}}(M_Z) &= m_c^{\overline{\rm MS}}(M_Z) \\ &\quad \times \left(1 - \frac{\alpha_s}{3\pi} - \frac{29\alpha_s^2}{72\pi^2} + \frac{3g_2^2}{128\pi^2} + \frac{g_1^2}{1920\pi^2}\right)_{\overline{\rm MS}}, \\ m_\tau^{\overline{\rm DR}}(M_Z) &= m_\tau^{\overline{\rm MS}}(M_Z)\left(1 + \frac{3g_2^2}{128\pi^2} - \frac{9g_1^2}{640\pi^2}\right)_{\overline{\rm MS}}. \end{aligned} \tag{B2}$$

For the lighter SM fermions these conversion corrections are neglected, i.e., we take $m_f^{\overline{\rm DR}} = m_f^{\overline{\rm MS}}$ at M_Z for $f = u, d, s, e, \mu$.

For the top quark, we obtain the running mass at $Q = m_t$ using the 2-loop QCD expression [78],

$$m_t^{\overline{\rm DR}}(m_t) = m_t\left[1 + \frac{5}{3}\frac{\alpha_s(m_t)}{\pi} + \left(\frac{\alpha_s(m_t)}{\pi}\right)^2 \Sigma_t^{\text{2-loop}}\right], \tag{B3}$$

where $\Sigma_t^{\text{2-loop}}$ is the 2-loop piece. Note that we activate the top quark at the scale of its mass, so we have a 5-flavor scheme below $Q = m_t$ and all 6 flavors above it.

The obtained $\overline{\rm DR}$ values of SM fermion masses are then substituted into Eq. (A3) to calculate the Yukawa matrices at M_Z in the gauge eigenbasis. A choice of basis is made by specifying fermion rotation matrices $\mathbf{V}_\bullet$ defined in

TABLE VI. SM input parameters [72] for ISAJET-M. All masses are in GeV and $\delta^{\rm CKM}$ is in radians.

Parameter	Value	Parameter	Value
M_Z	91.1876	m_t	171
$1/\alpha^{\overline{\rm MS}}(M_Z)$	127.918	$m_b - m_c$	3.42
$\alpha_s^{\overline{\rm MS}}(M_Z)$	0.1176	$m_e \times 10^3$	0.511
$\sin^2\theta_W(M_Z)$	0.23122	m_μ	0.105 66
m_u(2 GeV)	0.003	m_τ	1.776 99
m_d(2 GeV)	0.006	$\sin\theta_{12}^{\rm CKM}$	0.227 15
m_s(2 GeV)	0.095	$\sin\theta_{23}^{\rm CKM}$	0.041 61
$m_c(m_c)^{\overline{\rm MS}}$	1.25	$\sin\theta_{13}^{\rm CKM}$	0.003 682
$m_b(m_b)^{\overline{\rm MS}}$	4.20	$\delta^{\rm CKM}$	1.0884

Eq. (A3). ISAJET-M also has options for performing calculations in the unmixed and dominant third-family approximations.

The obtained weak-scale values of gauge couplings and Yukawa matrices are evolved to the grand unification scale $M_{\rm Gut}$ via MSSM RGEs in the $\overline{\rm DR}$ scheme. The GUT scale $M_{\rm Gut}$ is defined to be the scale at which $g_1 = g_2$, where $g_1 = \sqrt{5/3}g'$ is the hypercharge coupling in the GUT-scale normalization. We do not impose an exact unification of the strong coupling ($g_3 = g_1 = g_2$) at $M_{\rm Gut}$, assuming that the resulting few percent discrepancy comes from GUT-scale threshold corrections [79].

For the evolution of gauge and Yukawa couplings, we use a multiscale effective theory approach proposed in Ref. [80], where heavy degrees of freedom are integrated out at each particle threshold. In Appendix C, we list the corrected Yukawa 1-loop RGEs from an unpublished erratum of Ref. [80]. In the second-loop RGE terms we change from MSSM formulae [81] to SM expressions [60,69] at a single scale, $Q = M_{\rm SUSY} \equiv \sqrt{m_{\tilde{t}_L} m_{\tilde{t}_R}}$, thus introducing an error of 3-loop order that is negligible.

This ''step beta-function approach'' produces continuous matching conditions across thresholds. However, decoupling of a heavy particle also introduces finite shifts in RGE parameters [82]; a similar effect has long been known in QCD, where the decoupling of heavy quarks leads to shifts in the running masses of the light quarks [83]. Expressions for shifts induced by decoupling of each individual sparticle depend on the ordering of sparticle spectrum and are not yet known for the general case. Therefore, we implement these sparticle-induced finite shifts (to all three generations) collectively at a common scale $Q = M_{\rm SUSY}$ in the basis where Yukawa matrices are diagonal; we use 1-loop expressions of Ref. [84] without logarithmic terms that have already been resummed by the RGE evolution. For the top Yukawa coupling additional 2-loop SUSY-QCD corrections are included according to Ref. [78]. These finite threshold corrections are particularly important for GUT theories since they change ratios of Yukawa couplings from those at the weak scale, as was emphasized in Ref. [85]. This multiscale approach is a generalization of the one used by the standard ISAJET, as is described in detail in Ref. [86], and is preferred to single-scale decoupling when the sparticle mass hierarchy is large (as appears, for example, in the HB/FP region [28] of mSUGRA).

At $M_{\rm Gut}$, the SSB boundary conditions are imposed and all SSB parameters along with gauge and Yukawa couplings are evolved back down to the weak scale M_Z. For the SSB parameters we use 2-loop RGEs from Ref. [81] with the following conversion between notations: $\mathbf{f}_\bullet \equiv \mathbf{Y}_\bullet^T$, $\mathbf{a}_\bullet \equiv -\mathbf{h}_\bullet^T$, $b \equiv -B$. Unlike the gauge and Yukawa couplings, where beta functions change at every threshold, the SSB beta functions remain those of the MSSM all the way down to M_Z. We do not take into account threshold effects from the appearance of new couplings in the region of broken supersymmetry introduced in Refs. [68,69]. The entire parameter set is iteratively run between M_Z and $M_{\rm Gut}$ using full 2-loop RGEs in matrix form until a stable solution is obtained. After each iteration the Higgs potential is minimized and sparticle/Higgs masses are recalculated. The obtained mass spectrum is used in the next iteration to appropriately account for sparticle threshold effects on the RGE evolution.

The minimization of the RGE-improved potential is done using the tadpole method [87]. We include 1-loop contributions from third generation sfermions, which dominate, as well as contributions from charginos, neutralinos, and Higgs bosons. Computation is done at an optimized scale $Q = M_{\rm SUSY}$, which effectively accounts for the leading 2-loop corrections. Since tadpoles that contribute to μ and b strongly depend on the parameters themselves, an iterative procedure is employed. Calculations of μ, b and tadpoles are iterated until consistent values with a precision of 0.1% are obtained; usually this requires 3–4 iterations.

In the computation of sparticle masses we use SSB parameters extracted at their respective mass scales. Then, the SSB matrices are assembled and rotated to the SCKM basis as in Eq. (A7). The resultant matrices are plugged into the sfermion mass-squared matrices (A6). Instead of diagonalizing the full 6×6 matrices (A6) we diagonalize three 2×2 submatrices, thereby neglecting intragenerational mixings, which are required to be small by experimental limits on flavor-changing neutral current processes [33]. For the finite corrections, the full expressions of Ref. [84] for 1-loop self-energies are used.

For the SUSY seesaw we also use the multiscale approach that is mandatory to obtain correct values in the neutrino sector in the case of hierarchical RHNs [88]. Our approach is identical to the one used in the REAP code [61]. Above the scale of the heaviest RHN we have a full MSSM + RHN setup, with the MSSM RGEs extended to include full 2-loop equations for $\mathbf{f}_\nu$, $\mathbf{a}_\nu$, $\mathbf{m}^2_{\tilde{\nu}_{\mathbf{R}}}$ and $\mathbf{M}_N$ [10,18]. As mentioned earlier, bilinear coupling matrix $\mathbf{b}_\nu$ only introduces mixings for right-handed sneutrino states whose masses are $\mathcal{O}(M_{\rm Maj})$ and is thus irrelevant for our analysis. We also take into account additional contributions to RGEs of ordinary MSSM parameters due to the RHN superfields up to 2-loop order [10,18,61,89]. For large neutrino Yukawa couplings these additional RGE terms cause changes to the MSSM sparticle spectrum that can have significant consequences for experimental rates [31,32]. Below the scale of the lightest RHN, the RGEs are those of the MSSM, plus additional equations for the coupling κ of the dimension-five effective neutrino operator (A11) that are included at 2-loop level [61]. In the intermediate region, both κ and some elements of $\mathbf{f}_\nu$ and $\mathbf{M}_N$ are present. Transitions between them are done using matching conditions at RHN thresholds Eq. (A12). We

match only at tree-level and neglect small finite threshold corrections. The position of RHN thresholds M_{N_k} are determined by the eigenvalues of the RGE-evolving Majorana mass matrix $\mathbf{M}_N$ at those scales. Note that Eq. (A12) is valid only in the basis where $\mathbf{M}_N$ is diagonal at the threshold, which is different from the original basis at $M_{\rm Gut}$ due to RGE effects. Below the scale $Q = M_{N_k}$, the k-th RHN superfields are absent from the theory so we remove the corresponding columns of $\mathbf{f}_\nu$ and $\mathbf{a}_\nu$ matrices and the k-th row and column of $\mathbf{m}^2_{\tilde{\nu}_\mathbf{R}}$ and $\mathbf{M}_N$ in the basis where $\mathbf{M}_N$ is diagonal.

Since some of the RGE parameters (gauge and Yukawa couplings) are defined at the weak scale, while the rest are set at $M_{\rm Gut}$, an iterative procedure is employed to solve the RGEs. Once a stable solution to the RGEs is obtained, the decay width and branching ratios for all the sparticles and Higgs bosons are calculated. This step as well as the previous computation of the mass spectrum is performed using standard ISAJET subroutines [55]. A graphical outline of our code, for a SUSY-seesaw model that uses top-down approach for the neutrino sector (i.e., $\mathbf{f}_\nu$, $\mathbf{M}_N$ are inputted at the GUT scale and physical light neutrino masses and mixing parameters are derived results), is shown in Fig. 1.

ISAJET-M has the facility to calculate and return the neutralino relic density $\Omega_{\tilde{Z}_1}h^2$, neutralino-nucleon elastic cross sections, branching fractions for $b \to s\gamma$ and $B_s \to \mu\mu/\tau\tau$ decays, and supersymmetric contributions to the muon anomalous magnetic moment $\Delta a_\mu \equiv (g-2)_\mu/2$. These computations are done, respectively, by the IsaReD [26], IsaReS [90], IsaBSG [91], IsaBMM [92] and IsaAMU [58] codes from the ISATOOLS package. In addition, for scenarios with massive neutrinos, branching fractions for lepton flavor-violating decays $l_i \to l_j\gamma$ and $l_i \to 3l_j$ as well as rates for $\mu \to e$ conversion in several nuclei can be calculated using expressions from Ref. [12].

APPENDIX C: YUKAWA RGES

The following are the 1-loop RGEs for MSSM Yukawa coupling matrices with sparticle/Higgs thresholds from Ref. [80] with corrections from their unpublished erratum implemented:

$$
\begin{aligned}
(4\pi)^2\frac{d(\mathbf{f}_u^T)_{ij}}{dt} &= \frac{3}{2}(s^2\theta_h + c^2\theta_H)(\mathbf{f}_u^T\mathbf{f}_u^*\mathbf{f}_u^T)_{ij} + \frac{1}{2}(c^2\theta_{\tilde{h}} + s^2\theta_{\tilde{H}})\sum_{k=1}^{N_{\tilde{d}}}(\mathbf{f}_d^T)_{ik}(\mathbf{f}_d^*)_{kl}(\mathbf{f}_u^T)_{lj} + \frac{1}{2}(s^2\theta_{\tilde{h}} + c^2\theta_{\tilde{H}})\Bigg[2(\mathbf{f}_u^T)_{il}\sum_{k=1}^{N_{\tilde{Q}}}(\mathbf{f}_u^*)_{lk}(\mathbf{f}_u^T)_{kj} \\
&\quad + \sum_{k=1}^{N_{\tilde{u}}}(\mathbf{f}_u^T)_{ik}(\mathbf{f}_u^*)_{kl}(\mathbf{f}_u^T)_{lj}\Bigg] + \frac{1}{2}(c^2\theta_h + s^2\theta_H - 4c^2(\theta_h - \theta_H))(\mathbf{f}_d^T\mathbf{f}_d^*\mathbf{f}_u^T)_{ij} + (\mathbf{f}_u^T)_{ij}[(s^2\theta_h + c^2)\,\mathrm{Tr}\{3\mathbf{f}_u^*\mathbf{f}_u^T\} \\
&\quad + c^2(\theta_h - 1)\,\mathrm{Tr}\{3\mathbf{f}_d^*\mathbf{f}_d^T + \mathbf{f}_e^*\mathbf{f}_e^T\}] - (\mathbf{f}_u^T)_{ij}\Bigg[\frac{3}{5}g_1^2\Bigg\{\frac{17}{12} + \frac{3}{4}\theta_{\tilde{h}} - \Big(\frac{1}{36}\theta_{\tilde{Q}_j} + \frac{4}{9}\theta_{\tilde{u}_i} + \frac{1}{4}\theta_{\tilde{h}}\Big)\theta_{\tilde{B}}\Bigg\} \\
&\quad + g_2^2\Bigg\{\frac{9}{4} + \frac{9}{4}\theta_{\tilde{h}} - \frac{3}{4}(\theta_{\tilde{Q}_j} + \theta_{\tilde{h}})\theta_{\tilde{W}}\Bigg\} + g_3^2\Bigg\{8 - \frac{4}{3}(\theta_{\tilde{Q}_j} + \theta_{\tilde{u}_i})\theta_{\tilde{g}}\Bigg\}\Bigg], \\
(4\pi)^2\frac{d(\mathbf{f}_d^T)_{ij}}{dt} &= \frac{3}{2}(c^2\theta_h + s^2\theta_H)(\mathbf{f}_d^T\mathbf{f}_d^*\mathbf{f}_d^T)_{ij} + \frac{1}{2}(s^2\theta_{\tilde{h}} + c^2\theta_{\tilde{H}})\sum_{k=1}^{N_{\tilde{u}}}(\mathbf{f}_u^T)_{ik}(\mathbf{f}_u^*)_{kl}(\mathbf{f}_d^T)_{lj} + \frac{1}{2}(c^2\theta_{\tilde{h}} + s^2\theta_{\tilde{H}}) \\
&\quad \times\Bigg[2(\mathbf{f}_d^T)_{il}\sum_{k=1}^{N_{\tilde{Q}}}(\mathbf{f}_d^*)_{lk}(\mathbf{f}_d^T)_{kj} + \sum_{k=1}^{N_{\tilde{d}}}(\mathbf{f}_d^T)_{ik}(\mathbf{f}_d^*)_{kl}(\mathbf{f}_d^T)_{lj}\Bigg] + \frac{1}{2}(s^2\theta_h + c^2\theta_H - 4s^2(\theta_h - \theta_H))(\mathbf{f}_u^T\mathbf{f}_u^*\mathbf{f}_d^T)_{ij} \\
&\quad + (\mathbf{f}_d^T)_{ij}[s^2(\theta_h - 1)\,\mathrm{Tr}\{3\mathbf{f}_u^*\mathbf{f}_u^T\} + (c^2\theta_h + s^2)\,\mathrm{Tr}\{3\mathbf{f}_d^*\mathbf{f}_d^T + \mathbf{f}_e^*\mathbf{f}_e^T\}] - (\mathbf{f}_d^T)_{ij}\Bigg[\frac{3}{5}g_1^2\Bigg\{\frac{5}{12} + \frac{3}{4}\theta_{\tilde{h}} \\
&\quad - \Big(\frac{1}{36}\theta_{\tilde{Q}_j} + \frac{1}{9}\theta_{\tilde{d}_i} + \frac{1}{4}\theta_{\tilde{h}}\Big)\theta_{\tilde{B}}\Bigg\} + g_2^2\Bigg\{\frac{9}{4} + \frac{9}{4}\theta_{\tilde{h}} - \frac{3}{4}(\theta_{\tilde{Q}_j} + \theta_{\tilde{h}})\theta_{\tilde{W}}\Bigg\} + g_3^2\Bigg\{8 - \frac{4}{3}(\theta_{\tilde{Q}_j} + \theta_{\tilde{d}_i})\theta_{\tilde{g}}\Bigg\}\Bigg], \\
(4\pi)^2\frac{d(\mathbf{f}_e^T)_{ij}}{dt} &= \frac{3}{2}(c^2\theta_h + s^2\theta_H)(\mathbf{f}_e^T\mathbf{f}_e^*\mathbf{f}_e^T)_{ij} + \frac{1}{2}(c^2\theta_{\tilde{h}} + s^2\theta_{\tilde{H}})\Bigg[2(\mathbf{f}_e^T)_{il}\sum_{k=1}^{N_{\tilde{L}}}(\mathbf{f}_e^*)_{lk}(\mathbf{f}_e^T)_{kj} + \sum_{k=1}^{N_{\tilde{e}}}(\mathbf{f}_e^T)_{ik}(\mathbf{f}_e^*)_{kl}(\mathbf{f}_e^T)_{lj}\Bigg] \\
&\quad + (\mathbf{f}_e^T)_{ij}[s^2(\theta_h - 1)\,\mathrm{Tr}\{3\mathbf{f}_u^*\mathbf{f}_u^T\} + (c^2\theta_h + s^2)\,\mathrm{Tr}\{3\mathbf{f}_d^*\mathbf{f}_d^T + \mathbf{f}_e^*\mathbf{f}_e^T\}] - (\mathbf{f}_e^T)_{ij}\Bigg[\frac{3}{5}g_1^2\Bigg\{\frac{15}{4} + \frac{3}{4}\theta_{\tilde{h}} \\
&\quad - \Big(\frac{1}{4}\theta_{\tilde{L}_j} + \theta_{\tilde{e}_i} + \frac{1}{4}\theta_{\tilde{h}}\Big)\theta_{\tilde{B}}\Bigg\} + g_2^2\Bigg\{\frac{9}{4} + \frac{9}{4}\theta_{\tilde{h}} - \frac{3}{4}(\theta_{\tilde{L}_j} + \theta_{\tilde{h}})\theta_{\tilde{W}}\Bigg\}\Bigg],
\end{aligned}
$$

where $s = \sin\alpha$, $c = \cos\alpha$, α is Higgs mixing angle and the various $\theta_{\mathcal{P}}$'s are equal to zero below the mass threshold of the respective particle and equal to one above it. The contributions from neutrino Yukawa couplings can be found in Refs. [10,18].

[1] For a review of neutrino oscillations, see e.g., V. Barger, D. Marfatia, and K. Whisnant, Int. J. Mod. Phys. E **12**, 569 (2003).

[2] T. Schwetz, M. Tortola, and J. W. F. Valle, New J. Phys. **10**, 113011 (2008).

[3] H. Fritzsch and P. Minkowski, Phys. Lett. **62B**, 72 (1976); P. Minkowski, Phys. Lett. **67B**, 421 (1977); M. Gell-Mann, P. Ramond, and R. Slansky, in *Supergravity: Proceedings of the Workshop at Stony Brook*, (North-Holland, Amsterdam, 1979); T. Yanagida, KEK Report No. 79-18, 1979; S. Glashow, in *Quarks and Leptons, Cargese, France* (Plenum, New York, 1980); R. N. Mohapatra and G. Senjanovic, Phys. Rev. Lett. **44**, 912 (1980).

[4] S. T. Petcov, Sov. J. Nucl. Phys. **25**, 340 (1977); **25**, 698(E) (1977); **25**, 1336(E) (1977); S. M. Bilenky, S. T. Petcov, and B. Pontecorvo, Phys. Lett. **67B**, 309 (1977); T. P. Cheng and L. F. Li, Phys. Rev. Lett. **45**, 1908 (1980); B. W. Lee, S. Pakvasa, R. E. Shrock, and H. Sugawara, Phys. Rev. Lett. **38**, 937 (1977); **38**, 1230(E) (1977); V. D. Barger and D. V. Nanopoulos, Nuovo Cimento Soc. Ital. Fis. A **44**, 303 (1978).

[5] H. Baer and X. Tata, *Weak Scale Supersymmetry: From Superfields to Scattering Events* (Cambridge University Press, Cambridge, England, 2006).

[6] M. Drees, R. Godbole, and P. Roy, *Theory and Phenomenology of Sparticles: An Account of Four-Dimensional $N = 1$ Supersymmetry in High Energy Physics* (World Scientific, Singapore, 2004); S. P. Martin, arXiv:hep-ph/9709356.

[7] C. S. Aulakh, A. Melfo, A. Rasin, and G. Senjanovic, Phys. Lett. B **459**, 557 (1999).

[8] J. A. Casas, V. Di Clemente, A. Ibarra, and M. Quiros, Phys. Rev. D **62**, 053005 (2000); J. A. Casas, J. R. Espinosa, and I. Hidalgo, J. High Energy Phys. 11 (2004) 057.

[9] L. Girardello and M. T. Grisaru, Nucl. Phys. **B194**, 65 (1982).

[10] J. A. Casas and A. Ibarra, Nucl. Phys. **B618**, 171 (2001).

[11] A. Masiero, S. K. Vempati, and O. Vives, Nucl. Phys. **B649**, 189 (2003).

[12] J. Hisano, T. Moroi, K. Tobe, M. Yamaguchi, and T. Yanagida, Phys. Lett. B **357**, 579 (1995); J. Hisano, T. Moroi, K. Tobe, and M. Yamaguchi, Phys. Rev. D **53**, 2442 (1996).

[13] J. Hisano and D. Nomura, Phys. Rev. D **59**, 116005 (1999).

[14] S. T. Petcov, S. Profumo, Y. Takanishi, and C. E. Yaguna, Nucl. Phys. **B676**, 453 (2004).

[15] K. S. Babu and C. Kolda, Phys. Rev. Lett. **89**, 241802 (2002); A. Dedes, J. R. Ellis, and M. Raidal, Phys. Lett. B **549**, 159 (2002); R. Kitano, M. Koike, S. Komine, and Y. Okada, Phys. Lett. B **575**, 300 (2003).

[16] E. Arganda and M. J. Herrero, Phys. Rev. D **73**, 055003 (2006); E. Arganda, M. J. Herrero, and A. M. Teixeira, J. High Energy Phys. 10 (2007) 104.

[17] S. Antusch, E. Arganda, M. J. Herrero, and A. M. Teixeira, J. High Energy Phys. 11 (2006) 090.

[18] A. Ibarra and C. Simonetto, J. High Energy Phys. 04 (2008) 102.

[19] D. F. Carvalho, J. R. Ellis, M. E. Gomez, and S. Lola, Phys. Lett. B **515**, 323 (2001); J. R. Ellis, J. Hisano, M. Raidal, and Y. Shimizu, Phys. Rev. D **66**, 115013 (2002); F. Deppisch, H. Pas, A. Redelbach, R. Ruckl, and Y. Shimizu, Eur. Phys. J. C **28**, 365 (2003); T. Blazek and S. F. King, Nucl. Phys. **B662**, 359 (2003); A. Masiero, S. K. Vempati, and O. Vives, New J. Phys. **6**, 202 (2004); A. Masiero, S. Profumo, S. K. Vempati, and C. E. Yaguna, J. High Energy Phys. 03 (2004) 046; S. T. Petcov, T. Shindou, and Y. Takanishi, Nucl. Phys. **B738**, 219 (2006); S. T. Petcov, W. Rodejohann, T. Shindou, and Y. Takanishi, Nucl. Phys. **B739**, 208 (2006); F. Deppisch, H. Pas, A. Redelbach, and R. Ruckl, Phys. Rev. D **73**, 033004 (2006); L. Calibbi, A. Faccia, A. Masiero, and S. K. Vempati, Phys. Rev. D **74**, 116002 (2006); S. Antusch, E. Arganda, M. J. Herrero, and A. M. Teixeira, Nucl. Phys. B, Proc. Suppl. **169**, 155 (2007); S. Antusch and S. F. King, Phys. Lett. B **659**, 640 (2008); A. Ibarra, T. Shindou, and C. Simonetto, J. High Energy Phys. 10 (2008) 021.

[20] For reviews, see e.g. G. Jungman, M. Kamionkowski, and K. Griest, Phys. Rep. **267**, 195 (1996); A. B. Lahanas, N. E. Mavromatos, and D. V. Nanopoulos, Int. J. Mod. Phys. D **12**, 1529 (2003); M. Drees, arXiv:hep-ph/0410113; K. A. Olive, arXiv:astro-ph/0503065; Adv. Space Res. **42**, 581 (2008).

[21] E. Komatsu *et al.*, Astrophys. J. Suppl. Ser. **180**, 330 (2009); see also http://lambda.gsfc.nasa.gov/product/map/current/parameters.cfm.

[22] A. H. Chamseddine, R. L. Arnowitt, and P. Nath, Phys. Rev. Lett. **49**, 970 (1982); R. Barbieri, S. Ferrara, and C. A. Savoy, Phys. Lett. B **119**, 343 (1982); N. Ohta, Prog. Theor. Phys. **70**, 542 (1983); L. J. Hall, J. D. Lykken, and S. Weinberg, Phys. Rev. D **27**, 2359 (1983); for reviews, see H. P. Nilles, Phys. Rep. **110**, 1 (1984); P. Nath, arXiv:hep-ph/0307123.

[23] J. R. Ellis, J. S. Hagelin, D. V. Nanopoulos, K. A. Olive, and M. Srednicki, Nucl. Phys. **B238**, 453 (1984); V. D. Barger and C. Kao, Phys. Rev. D **57**, 3131 (1998).

[24] H. Baer and M. Brhlik, Phys. Rev. D **53**, 597 (1996).

[25] J. R. Ellis, T. Falk, and K. A. Olive, Phys. Lett. B **444**, 367 (1998); J. R. Ellis, T. Falk, K. A. Olive, and M. Srednicki, Astropart. Phys. **13**, 181 (2000); **15**, 413(E) (2001); M. E. Gomez, G. Lazarides, and C. Pallis, Phys. Rev. D **61**, 123512 (2000); Phys. Lett. B **487**, 313 (2000); A. B. Lahanas, D. V. Nanopoulos, and V. C. Spanos, Phys. Rev. D **62**, 023515 (2000); R. L. Arnowitt, B. Dutta, and Y. Santoso, Nucl. Phys. **B606**, 59 (2001).

[26] H. Baer, C. Balazs, and A. Belyaev, J. High Energy Phys. 03 (2002) 042.

[27] C. Boehm, A. Djouadi, and M. Drees, Phys. Rev. D **62**, 035012 (2000); J. R. Ellis, K. A. Olive, and Y. Santoso, Astropart. Phys. **18**, 395 (2003); J. Edsjo, M. Schelke, P. Ullio, and P. Gondolo, J. Cosmol. Astropart. Phys. 04 (2003) 001.

[28] K. L. Chan, U. Chattopadhyay, and P. Nath, Phys. Rev. D **58**, 096004 (1998); J. L. Feng, K. T. Matchev, and T. Moroi, Phys. Rev. Lett. **84**, 2322 (2000); Phys. Rev. D **61**, 075005 (2000); H. Baer, C. h. Chen, F. Paige, and X. Tata, Phys. Rev. D **52**, 2746 (1995); **53**, 6241 (1996); H. Baer, C. h. Chen, M. Drees, F. Paige, and X. Tata, Phys. Rev. D **59**, 055014 (1999).

[29] M. Drees and M. M. Nojiri, Phys. Rev. D **47**, 376 (1993); H. Baer and M. Brhlik, Phys. Rev. D **57**, 567 (1998); H. Baer, M. Brhlik, M. A. Diaz, J. Ferrandis, P. Mercadante, P. Quintana, and X. Tata, Phys. Rev. D **63**, 015007 (2000); J. R. Ellis, T. Falk, G. Ganis, K. A. Olive, and M. Srednicki, Phys. Lett. B **510**, 236 (2001); L. Roszkowski, R. Ruiz de Austri, and T. Nihei, J. High Energy Phys. 08 (2001) 024; A. Djouadi, M. Drees, and J. L. Kneur, J. High Energy Phys. 08 (2001) 055; A. B. Lahanas and V. C. Spanos, Eur. Phys. J. C **23**, 185 (2002).

[30] P. Nath and R. L. Arnowitt, Phys. Rev. Lett. **70**, 3696 (1993); A. Djouadi, M. Drees, and J. L. Kneur, Phys. Lett. B **624**, 60 (2005).

[31] H. Baer, C. Balazs, J. K. Mizukoshi, and X. Tata, Phys. Rev. D **63**, 055011 (2001).

[32] V. Barger, D. Marfatia, and A. Mustafayev, Phys. Lett. B **665**, 242 (2008).

[33] M. Ciuchini, A. Masiero, P. Paradisi, L. Silvestrini, S. K. Vempati, and O. Vives, Nucl. Phys. **B783**, 112 (2007).

[34] M. L. Brooks *et al.* (MEGA Collaboration), Phys. Rev. Lett. **83**, 1521 (1999).

[35] S. Ritt (MEG Collaboration), Nucl. Phys. B, Proc. Suppl. **162**, 279 (2006); T. Mori, Nucl. Phys. B, Proc. Suppl. **169**, 166 (2007).

[36] K. Hayasaka *et al.* (Belle Collaboration), Phys. Lett. B **666**, 16 (2008).

[37] M. Bona *et al.*, arXiv:0709.0451; A. G. Akeroyd *et al.* (SuperKEKB Physics Working Group), arXiv:hep-ex/0406071.

[38] B. Aubert *et al.* (*BABAR* Collaboration), arXiv:0908.2381.

[39] U. Bellgardt *et al.* (SINDRUM Collaboration), Nucl. Phys. **B299**, 1 (1988).

[40] With no experiment planned, we use theoretical estimates based on the PSI beam intensity from W. J. Marciano, T. Mori, and J. M. Roney, Annu. Rev. Nucl. Part. Sci. **58**, 315 (2008).

[41] Y. Miyazaki *et al.* (Belle Collaboration), Phys. Lett. B **660**, 154 (2008).

[42] C. Dohmen *et al.* (SINDRUM II Collaboration), Phys. Lett. B **317**, 631 (1993).

[43] Y. Mori *et al.* (The PRIME Working Group), http://www-ps.kek.jp/jhf-np/LOIlist/LOIlist.html.

[44] E. C. Dukes *et al.* (Mu2e Collaboration), http://mu2e.fnal.gov/public/hep/index.shtml.

[45] See e.g., A. Belyaev, S. Dar, I. Gogoladze, A. Mustafayev, and Q. Shafi, arXiv:0712.1049.

[46] H. C. Chiang, E. Oset, T. S. Kosmas, A. Faessler, and J. D. Vergados, Nucl. Phys. **A559**, 526 (1993).

[47] A. Czarnecki, W. J. Marciano, and K. Melnikov, AIP Conf. Proc. **435**, 409 (1998); R. Kitano, M. Koike, and Y. Okada, Phys. Rev. D **66**, 096002 (2002); **76**, 059902(E) (2007).

[48] T. Suzuki, D. F. Measday, and J. P. Roalsvig, Phys. Rev. C **35**, 2212 (1987).

[49] R. N. Mohapatra and A. Y. Smirnov, Annu. Rev. Nucl. Part. Sci. **56**, 569 (2006); C. H. Albright and M. C. Chen, Phys. Rev. D **74**, 113006 (2006).

[50] R. N. Mohapatra and B. Sakita, Phys. Rev. D **21**, 1062 (1980).

[51] P. F. Harrison, D. H. Perkins, and W. G. Scott, Phys. Lett. B **530**, 167 (2002); Z. z. Xing, Phys. Lett. B **533**, 85 (2002); X. G. He and A. Zee, Phys. Lett. B **560**, 87 (2003).

[52] P. F. Harrison and W. G. Scott, Phys. Lett. B **535**, 163 (2002).

[53] C. H. Albright, Phys. Lett. B **599**, 285 (2004).

[54] C. H. Albright, arXiv:0905.0146.

[55] ISAJET, by H. Baer, F. Paige, S. Protopopescu, and X. Tata, arXiv:hep-ph/0312045.

[56] G. W. Bennett *et al.* (Muon (g-2) Collaboration), Phys. Rev. D **80**, 052008 (2009).

[57] A. Czarnecki and W. J. Marciano, Phys. Rev. D **64**, 013014 (2001); S. Komine, T. Moroi, and M. Yamaguchi, Phys. Lett. B **506**, 93 (2001).

[58] H. Baer, C. Balazs, J. Ferrandis, and X. Tata, Phys. Rev. D **64**, 035004 (2001).

[59] Tevatron Electroweak Working Group, CDF Collaboration, and D0 Collaboration, arXiv:0903.2503.

[60] V. D. Barger, M. S. Berger, and P. Ohmann, Phys. Rev. D **47**, 1093 (1993).

[61] S. Antusch, J. Kersten, M. Lindner, M. Ratz, and M. A. Schmidt, J. High Energy Phys. 03 (2005) 024.

[62] X. Guo *et al.* (Daya Bay Collaboration), arXiv:hep-ex/0701029.

[63] F. Ardellier *et al.* (Double Chooz Collaboration), arXiv:hep-ex/0606025.

[64] LEP2 SUSY Working Group, http://lepsusy.web.cern.ch/lepsusy/www/inos_moriond01/charginos_pub.html.

[65] G. F. Giudice, A. Notari, M. Raidal, A. Riotto, and A. Strumia, Nucl. Phys. **B685**, 89 (2004); A. Abada, S. Davidson, A. Ibarra, F. X. Josse-Michaux, M. Losada, and A. Riotto, J. High Energy Phys. 09 (2006) 010.

[66] P. Di Bari and A. Riotto, Phys. Lett. B **671**, 462 (2009).

[67] N. Cabibo, Phys. Rev. Lett. **10**, 531 (1963); M. Kobayashi and T. Maskawa, Prog. Theor. Phys. **49**, 652 (1973).

[68] A. D. Box and X. Tata, Phys. Rev. D **77**, 055007 (2008); **79**, 035004 (2009).

[69] A. D. Box, arXiv:0811.2444.

[70] L. J. Hall, V. A. Kostelecky, and S. Raby, Nucl. Phys. **B267**, 415 (1986).

[71] Z. Maki, M. Nakagawa, and S. Sakata, Prog. Theor. Phys. **28**, 870 (1962).

[72] C. Amsler *et al.* (Particle Data Group), Phys. Lett. B **667**, 1 (2008).

[73] H. Arason, D. J. Castano, B. Keszthelyi, S. Mikaelian, E. J. Piard, P. Ramond, and B. D. Wright, Phys. Rev. D **46**, 3945 (1992).

[74] O. V. Tarasov, A. A. Vladimirov, and A. Y. Zharkov, Phys. Lett. **93B**, 429 (1980); S. G. Gorishnii, A. L. Kataev, and S. A. Larin, Yad. Fiz. **40**, 517 (1984) [Sov. J. Nucl. Phys. **40**, 329 (1984)].

[75] K. G. Chetyrkin, B. A. Kniehl, and M. Steinhauser, Phys. Rev. Lett. **79**, 2184 (1997); Nucl. Phys. **B510**, 61 (1998).

[76] L. V. Avdeev and M. Y. Kalmykov, Nucl. Phys. **B502**, 419 (1997).

[77] S. P. Martin and M. T. Vaughn, Phys. Lett. B **318**, 331 (1993).

[78] A. Bednyakov, A. Onishchenko, V. Velizhanin, and O. Veretin, Eur. Phys. J. C **29**, 87 (2003).

[79] J. Hisano, H. Murayama, and T. Yanagida, Nucl. Phys. **B402**, 46 (1993); Y. Yamada, Z. Phys. C **60**, 83 (1993).

[80] D. J. Castano, E. J. Piard, and P. Ramond, Phys. Rev. D **49**, 4882 (1994).

[81] S. P. Martin and M. T. Vaughn, Phys. Rev. D **50**, 2282

(1994).
[82] S. Weinberg, Phys. Lett. **91B**, 51 (1980); L. J. Hall, Nucl. Phys. **B178**, 75 (1981); B. A. Ovrut and H. J. Schnitzer, Phys. Lett. **100B**, 403 (1981); Nucl. Phys. **B179**, 381 (1981).
[83] W. Wetzel, Nucl. Phys. **B196**, 259 (1982).
[84] D. M. Pierce, J. A. Bagger, K. T. Matchev, and R. j. Zhang, Nucl. Phys. **B491**, 3 (1997).
[85] G. Ross and M. Serna, Phys. Lett. B **664**, 97 (2008).
[86] H. Baer, J. Ferrandis, S. Kraml, and W. Porod, Phys. Rev. D **73**, 015010 (2006).
[87] P. H. Chankowski, S. Pokorski, and J. Rosiek, Nucl. Phys. **B423**, 437 (1994); V. D. Barger, M. S. Berger, and P. Ohmann, Phys. Rev. D **49**, 4908 (1994).
[88] S. Antusch, J. Kersten, M. Lindner, and M. Ratz, Phys. Lett. B **538**, 87 (2002).
[89] J. A. Casas, J. R. Espinosa, A. Ibarra, and I. Navarro, Phys. Rev. D **63**, 097302 (2001).
[90] H. Baer, C. Balazs, A. Belyaev, and J. O'Farrill, J. Cosmol. Astropart. Phys. 09 (2003) 007.
[91] H. Baer and M. Brhlik, Phys. Rev. D **55**, 3201 (1997); H. Baer, M. Brhlik, D. Castano, and X. Tata, Phys. Rev. D **58**, 015007 (1998).
[92] J. K. Mizukoshi, X. Tata, and Y. Wang, Phys. Rev. D **66**, 115003 (2002).
[93] M. Apollonio *et al.* (CHOOZ Collaboration), Eur. Phys. J. C **27**, 331 (2003).